81. Double-Diamond Inclusion Compounds of 2,6-Dimethylideneadamantane-1,3,5,7-tetracarboxylic Acid

by **Otto Ermer*** and **Lorenz Lindenberg**

Institut für Organische Chemie der Universität, Greinstrasse 4, D–5000 Köln 41

(28.II.91)

The crystal structures of four inclusion compounds of 2,6-dimethylideneadamantane-1,3,5,7-tetracarboxylic acid (**4**) are described, which involve the following guest species: *a*) a mixture of 4-methylpent-3-en-2-one, 2,6-dimethylhepta-2,5-dien-4-one, and mesitylene (condensation products of acetone); *b*) mesitylene; *c*) a mixture of 4-methylpent-3-en-2-one and mesitylene; *d*) (*tert*-butyl)benzene. In all four cases, the host architectures consist of two interpenetrating super-diamond networks built up by the tetra-acid molecules *via* pairwise H-bonds between the tetrahedrally directed COOH groups. In the first three cases (tetragonal crystal symmetry), the two diamond-like host lattices interpenetrate symmetrically, in the fourth case (monoclinic) asymmetrically. This asymmetry is brought about by the increased steric bulk of the (*tert*-butyl)benzene guest molecules. Attempts to enforce an inclusion compound of **4** with a single, extremely hollow diamond-like host lattice by offering still bulkier guest molecules have as yet not been met with success. The generally very high propensity of **4** to form inclusion compounds was envisaged and designed beforehand by appropriate evaluation and modulation of the crystal structure of the parent adamantane-1,3,5,7-tetracarboxylic acid, which represents a fivefold diamond-like self-inclusion compound. Crystals of the free, uncomplexed **4** appear to be extremely unstable and could so far not be obtained. On the other hand, from aqueous solution a very stable monohydrate of **4** may be crystallized (**4**·H_2O), which was also subjected to X-ray analysis. The (triclinic) crystal structure of **4**·H_2O involves an interesting dichotomy inasmuch its pattern of H-bonding may be rationalized either in terms of a double, cross-linked super-zincblende (sphalerite) architecture, or as a system of porous, puckered 4-connected sheets, which interpenetrate each other pairwise and are cross-linked by the H_2O molecules. Various structure and (space group) symmetry characteristics of the supramolecular solid-state complexes reported here are highlighted by pointing out analogies with comparable structures retrieved from the literature.

Introduction. – Tetrahedral tetracarboxylic acids are capable of forming hollow super-diamond architectures held together by pairwise H-bonds between the COOH groups. A representative example is adamantane-1,3,5,7-tetracarboxylic acid **1** [1]. In the crystal, the very large empty spaces of the super-diamond networks of **1** are filled by four interpenetrating, translationally equivalent networks (fivefold-diamond structure). Thus, **1** may by viewed as a 'degenerate' inclusion compound or self-inclusion compound.

A small steric modulation of the adamantane core in **1** by introducing two oxo groups as in **2** prevents the fivefold interpenetration and leads to a propensity for inclusion of guest molecules, since lower degrees of interpenetration cannot be attained without holes. Accordingly, crystallisation of **2** (or rather the hydrate **3**) from AcOH solution furnished a novel type of solid-state inclusion compound consisting of three interpenetrating super-diamond networks, which accommodate AcOH guest molecules in triple-helical channels (**3**·AcOH) [2]. This molecular complex is at the same time a genuine inclusion compound and a self-inclusion compound.

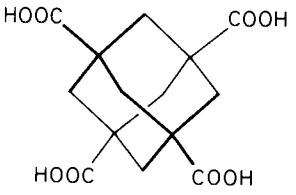

1

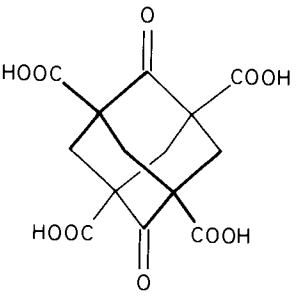

2

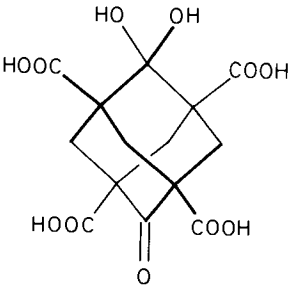

3

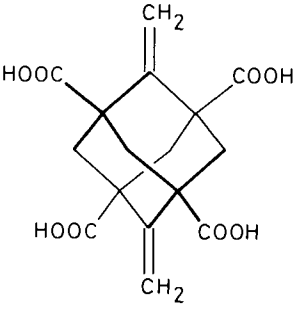

4

To probe the versatility of diamond-like host architectures in regard of the creation of larger cavities and thus the accommodation of more voluminous guest species, the 2,6-dimethylidene derivative **4** of adamantane-1,3,5,7-tetracarboxylic acid (**1**) was synthesized. This was easily accomplished through *Wittig* olefination of the tetramethyl ester of the dioxo-tetraacid **2** and subsequent hydrolysis (see *Experimental*). We sensed that the increased size of the methylidene groups in **4** (as compared to the oxo groups in **2**) should lead to a further reduction of the degree of interpenetration, most probably to a double super-diamond structure. This conjecture was further substantiated by the choice of acetone as guest molecules, which are somewhat bulkier than AcOH molecules. (Acetone was preferred to AcOH, since **4** is better soluble in the former.) A double-diamond-like architecture of **4** is of course substantially more hollow than the triple-diamond structure of **3** as evidenced by estimated densities of 0.72 and 1.16 $g \cdot cm^{-3}$, respectively. To attain a realistic density, one would expect **4** to include *ca.* 4 to 5 molecules of acetone per tetra-acid molecule, as compared to only 1.4 AcOH molecules by **3** [2].

The expected propensity of **4** to include molecular guests was quickly and rather dramatically confirmed in the course of initial attempts to crystallize the free tetra-acid from aqueous solution (neutralization with HCl of a solution of **4** in aqueous KOH; see *Experimental*). The crystals obtained turned out to be a monohydrate ($\mathbf{4} \cdot H_2O$) and remained unchanged, even when exposed for several months to P_2O_5 at a pressure of 0.1 Torr. We have thus far not been able to avoid the uptake of guest molecules and to crystallize free **4** from a variety of organic solvents.

The crystallization of an inclusion compound of **4** with acetone as guest species was attempted by dissolving **4**·H_2O in acetone and removal of the solvent (and H_2O) *via* the gas phase by means of P_2O_5 in a desiccator. The resulting crystals indeed consisted of a solid-state inclusion compound of **4**, yet to our surprise not with acetone as guest species but instead with a mixture of 4-methylpent-3-en-2-one (**5**, MP), 2,6-dimethylhepta-2,5-dien-4-one (**6**, DMH), and mesitylene (**7**, M; ratio **4**/**5**/**6**/**7** ≈ 1:0.6:0.1:1.1 as obtained by NMR analysis; see *Experimental*). Henceforth, we refer to this inclusion compound as **4**·(MP-DMH-M). Of course, **5**–**7** are volatile condensation products of acetone and are well-known to emerge from the latter in the presence of dehydrating agents. Notably, the crystals of **4**·(MP-DMH-M) did not contain detectable amounts of acetone or H_2O.

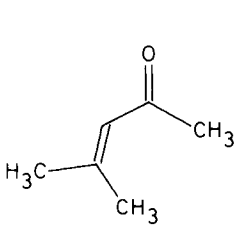

5 (MP)

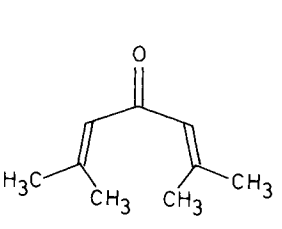

6 (DMH)

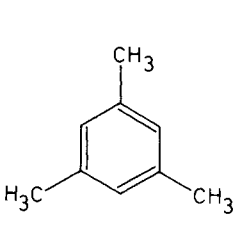

7 (M)

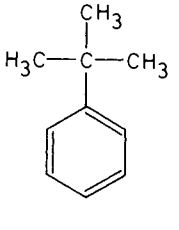

8 (TBB)

Apparently, under these dry crystallization conditions the otherwise tightly bound H_2O molecule of the monohydrate is readily displaced by **5**, **6**, and **7**. The above crystallization experiment was repeated several times and produced crystals of **4**·(MP-DMH-M) in all cases except one, which furnished different crystals of another inclusion compound of **4** with only **5** and **7** as molecular guests. These crystals devoid of **6** are labelled **4**·(MP-M) (ratio **4**/**5**/**7** ≈ 1:0.4:1.6; see *Experimental*). Subsequent crystal structure analyses showed that the guest molecules of **4**·(MP-DMH-M) are completely disordered and those of **4**·(MP-M) partly disordered. Closer inspection of the host-guest architecture of **4**·(MP-M) suggested the possibility that an inclusion compound of **4** exclusively with **7** as guest molecules could be crystallized with a ratio **4**/**7** = 1:2 in a fully ordered fashion. Accordingly, an inclusion compound of this nature was indeed obtained by performing the crystallization in the presence of an excess of **7** both in solution and the gas phase (see *Experimental*). In the following, the crystals of this third inclusion compound of host **4** are designated as **4**·M_2. We further concluded from the packing characteristics of **4**·(MP-M) and **4**·M_2 that replacement of the relatively flat, disc-shaped mesitylene guest, *e.g.* by the bulkier (*tert*-butyl)benzene molecule (**8**, TBB), should lead to a double-diamond architecture of the host **4** with asymmetric interpenetration or even to a single super-diamond host lattice, which would include an extremely large amount of guest molecules. Crystals of an inclusion compound of **4** with guest molecules **8** could indeed be grown and characterized crystallographically (ratio **4**/**8** ≈ 1:1.7) and are henceforth referred to as **4**·TBB.

As presumed and evidenced by X-ray analysis, the four crystallized inclusion compounds **4**·(MP-DMH-M), **4**·M_2, **4**·(MP-M), and **4**·TBB have double-diamond-like host architectures built up by doubly H-bonded molecules of the tetrahedral **4**. The two super-diamond host lattices interpenetrate symmetrically in the three inclusion compounds containing mesitylene (**7**) as guest species and asymmetrically in **4**·TBB. In the

following, the crystal structure analyses of these four rather unique diamond-like inclusion compounds are described in the above sequence, and their fascinating supramolecular architectures are characterized through various comparisons and illustrations.

Since **4**·H_2O may also favorably be described in terms of a (cross-linked) double-diamond or rather double-zincblende structure, its X-ray analysis and crystal structural properties are also reported here. Finally, it turned out that the crystal structure of **4**·H_2O may alternatively be viewed as a system of interpenetrating corrugated 4-connected sheets made up by the H-bonded tetracarboxylic-acid molecules, with the H_2O molecules interspersed between. The discussion of this intriguing aspect of the crystal architecture of **4**·H_2O will conclude our present report.

Experimental and Results. – *Preparation of 2,6-Dimethylideneadamantane-1,3,5,7-tetracarboxylic Acid* (**4**). Ylid preparation and *Wittig* reaction were carried out under dry Ar. To a slurry of 24.9 g (70 mmol) of methyltriphenylphosphonium bromide in 300 ml of abs. dioxane, an equivalent amount of BuLi dissolved in hexane is added. A soln. of 12.0 g of tetramethyl 2,6-dioxoadamantane-1,3,5,7-tetracarboxylate (O. Böttger, *Chem. Ber.* **1937,** *70,* 314) in 600 ml of dioxane is added dropwise (7 h, r.t., stirring) to the orange-yellow ylid soln. After stirring overnight and heating to 100° for 0.5 h, the yellow soln. is filtered and the solvent removed. The remaining syrup is digested with 300 ml of hot MeOH upon which the white crystalline product is precipitated. It is filtered off, washed with MeOH, and purified by boiling 3 h in 300 ml of MeOH (yield 6.9 g, 58%); identification of dried product as tetramethyl ester of **4** by IR, ^{1}H-NMR, and MS. The tetramethyl ester of **4** melts at 286° and is readily soluble in $CHCl_3$ and almost insoluble in MeOH. Well-developed octahedral crystals may be obtained by sublimation or from acetone soln. These tetra-ester crystals are body-centered tetragonal (*Laue* class 4/*m*) with cell constants $a = 10.881(1)$, $c = 16.240(2)$ Å. The measured density is $d_m = 1.38$ g·cm^{-3} indicating 4 molecules per unit cell ($d_x = 1.355$ g·cm^{-3}); no further X-ray structural work was performed on these crystals. It is noted that inverse performing of the *Wittig* reaction, *i.e.* adding the ylid to the dioxo-ester solution, furnished a 5:1 mixture of mono- and diolefinated products. The tetramethyl ester of **4** was hydrolyzed by NaOH in H_2O/MeOH (10 h reflux). Neutralization with dil. aq. HCl (ice cooling) precipitates the tetra-acid monohydrate **4**·H_2O, which is washed with H_2O and dried (P_2O_5) in a desiccator; characterization by IR, ^{1}H- and ^{13}C-NMR, MS, and finally X-ray spectroscopy (see below). The monohydrate **4**·H_2O decomposes beyond 340° (darkening); solubility is good in MeOH, DMSO, DMF, poor in acetone, and almost nil in hot H_2O. The H_2O-free inclusion compounds of **4** described subsequently are readily soluble in acetone.

Crystallographic Studies. Crystal and X-ray analytical data of the present inclusion compounds are collected in *Table 1.* Further related details may be found in abbreviated form in the following experimental accounts of the individual molecular complexes studied.

Inclusion Compound of **4** *with 4-Methylpent-3-en-2-one* (**5**), *2,6-Dimethylhepta-2,5-dien-4-one* (**6**), *and Mesitylene* (**7**) (**4**·(MP-DMH-M)). – The monohydrate **4**·H_2O was (slowly) dissolved in hot acetone and placed in a desiccator over P_2O_5 for solvent removal *via* the gas phase. The pale-yellow crystals precipitated after several days were clear and well-shaped according to (sometimes truncated) octahedra. They are sensitive to moisture and become blurred rather rapidly when exposed to normal atmospheric conditions.

Table 1. *Crystal Data and X-Ray Analytical Conditions of the Crystallographic Measurements.* The macroscopic densities d_m were measured by flotation in mixtures given in corresponding *Footnotes; no* d_m values measured for **4**·(MP-M) due to paucity of crystals. The reflection intensities were collected on a 4-circle diffractometer at r.t. throughout; Mo$K\alpha$ radiation was applied with $\lambda = 0.71069$ Å. The weighting scheme in the refinements took the form $w(F_o) = [\sigma^2(F_o) + pF_o^2]^{-1}$. Reflections with $F_o/\sigma(F_o) < [F_o/\sigma(F_o)]_{min}$ were excluded from refinement. N_{tot}, total number of reflections recorded; N_{indep}, total number of independent reflections; N_{ref}, number of reflections included in refinement; N_{var}, number of refinement variables; ρ_{res}, maximum residual electron density after refinement. See *Experimental* for further details.

Complex	**4**·(MP-DMH-M)	**4**·M_2	**4**·(MP-M)	**4**·TBB	**4**·H_2O
Composition	**4**·$\mathbf{5}_{0.6}$·$\mathbf{6}_{0.1}$·$\mathbf{7}_{1.1}$	**4**·$\mathbf{7}_2$	**4**·$\mathbf{5}_{0.4}$·$\mathbf{7}_{1.6}$	**4**·$\mathbf{8}_{1.7}$	
Crystal system	tetragonal	tetragonal	tetragonal	monoclinic	triclinic
Space group (origin on $\bar{1}$)	$P4_2/nnm$ (D_{4h}^{12}, No. 134)	$I4_1/acd$ (D_{4h}^{20}, No. 142)	$I4_1/acd$	$F2/d$ (see text)	$P\bar{1}$
Z	2	8	8	16	4
a [Å]	11.813(3)	16.195(3)	16.118(5)	23.518(3)	9.501(3)
b [Å]				22.808(7)	10.663(4)
c [Å]	10.934(2)	23.507(6)	23.558(7)	22.691(9)	16.265(6)
α [°]					94.95(3)
β [°]				91.46(2)	93.99(3)
γ [°]					108.74(3)
V [Å^3]	1525.8	6165.4	6120.1	12167	1546.3
d_x [g·cm^{-3}]	1.178	1.242	1.239	1.232	1.522
d_m [g·cm^{-3}]	1.24[a])	1.25[b])	–	1.26[c])	1.53[d])
θ_{max} [°]	27	28	27	27	27
θ_{min} [°]	13.3	–	–	13.3	–
N_{tot}	2128	4259	4137	7278	6725
N_{indep}	901	1864	1670	6614	6725
$[F_o/\sigma(F_o)]_{min}$	4	4	4	4	3
N_{ref}	208	770	651	2672	5595
N_{var}	35	117	115	219	595
ρ_{res} [eÅ^{-3}]	0.30	0.22	0.31	0.50	0.33
p	0.01	0.002	0.01	0.0008	0.0005
Total measuring time [h]	43	85	82	145	135
Crystal decay [%]	none	none	1.6	2.3	–0.6
R	0.102	0.049	0.066	0.117	0.045
R_w	0.109	0.051	0.073	0.112	0.053

[a]) CCl_4/(*tert*-butyl)benzene, CCl_4/mesitylene, CCl_4/cyclohexane. [b]) CCl_4/mesitylene. [c]) CH_2Br_2/(*tert*-butyl)-benzene. [d]) CCl_4/cyclohexane.

Most of the crystals corresponded to the complex **4**·(MP-DMH-M), whose composition and stoichiometry were analyzed by ^{1}H-NMR (**4**/**5**/**6**/**7** = 1:0.6:0.1:1.1). For the crystallographic measurements, the crystals of **4**·(MP-DMH-M) were mounted under dry conditions in capillaries, together with a drop of mother liquor and a bit of P_2O_5. Average crystallographic symmetry of the tetra-acid molecules D_{2d} (COOH groups with twofold torsional disorder); somewhat enhanced reflection backgrounds, possibly due to guest disorder; structure solution by direct methods, only tetra-acid atoms 'visible'; no sensible structural model for guest molecules derivable by difference *Fourier* techniques, guest molecules obviously more or less completely disordered; atomic parameters of host tetra-acid **4** only could thus be refined (C,O anisotropic, H-positions calculated and fixed, COOH H-atom not considered); 146 inner reflections with sin $\theta < 0.23$ excluded from refinement (*Table 1*); refinement on all 354 reflections with $F_o > 4\,\sigma(F_o)$, *i.e.* including

Table 2. *Refined Atomic Coordinates* ($\times 10^4$, hydrogen $\times 10^3$) *and Temperature Parameters* ($\times 10^3$) *of* **4**·*(MP-DMH-M)* (estimated standard deviations in parentheses). Anisotropic temperature factor expression, $\exp[-2\pi^2(U_{11}h^2a^{*2} + \cdots + 2U_{23}klb^*c^* + \cdots)]$; guest molecules disordered; for atomic numbering, see *Fig. 1b*.

	x	y	z	U_{11}	U_{22}	U_{33}	U_{23}	U_{13}	U_{12}
C(1)	8237(7)	$=1-x$	1665(9)	30(3)	$=U_{11}$	32(5)	0(3)	$=-U_{23}$	0(5)
C(2)	7500	2500	912(14)	28(4)	$=U_{11}$	28(8)	0	0	–17(6)
C(3)	7500	998(8)	2500	25(4)	25(5)	43(5)	0	6(4)	0
C(4)	7500	2500	–298(19)	62(7)	$=U_{11}$	45(10)	0	0	36(10)
C(5)	9018(8)	$=1-x$	893(12)	33(4)	$=U_{11}$	44(7)	1(4)	$=-U_{23}$	–12(5)
O	8652(7)	25(6)	615(9)	66(5)	45(4)	106(5)	–44(4)	–43(4)	–6(3)
H(3)	701	49	200	43					
H(4)	699	$=1-x$	–79	57					

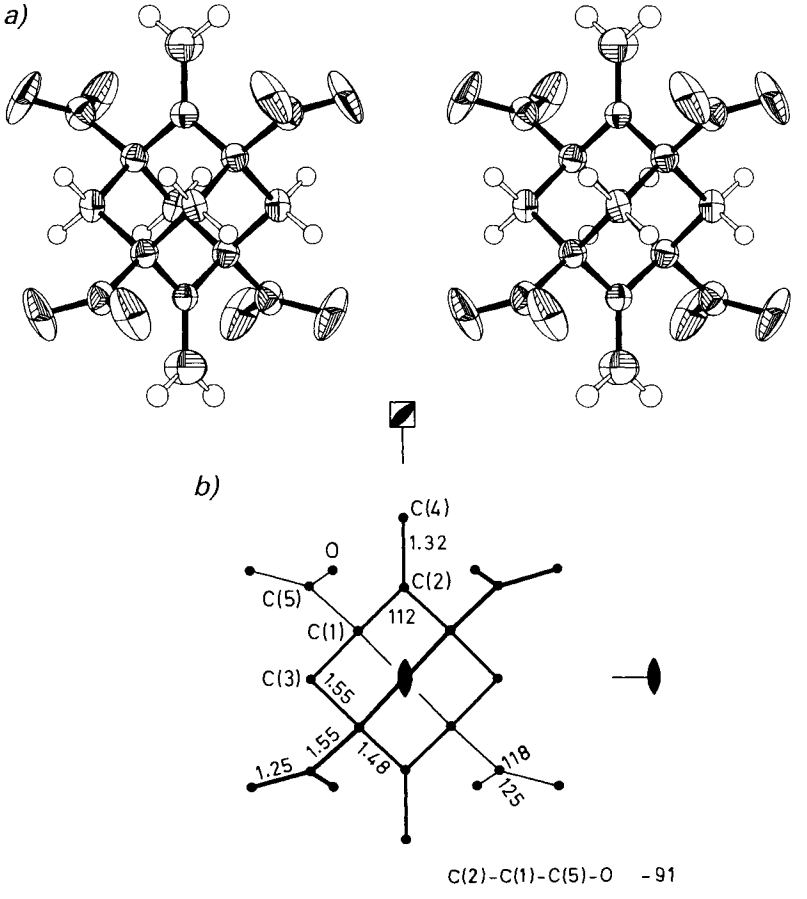

Fig. 1. *Crystal structure of* **4**·*(MP-DMH-M)* (molecular symmetry of host **4**, D_{2d}). a) *Stereoview of* **4** (along a C_2 axis for right member of pair) *with vibrational ellipsoids* (50% probability, U_{iso} of H-atoms divided by 3). b) *Atomic numbering and selected bond lengths* [Å], *bond angles, and torsion angle* [°]. Estimated average standard deviations *ca.* 0.02 Å and 1°, resp. The guest molecules of **4**·(MP-DMH-M) are disordered.

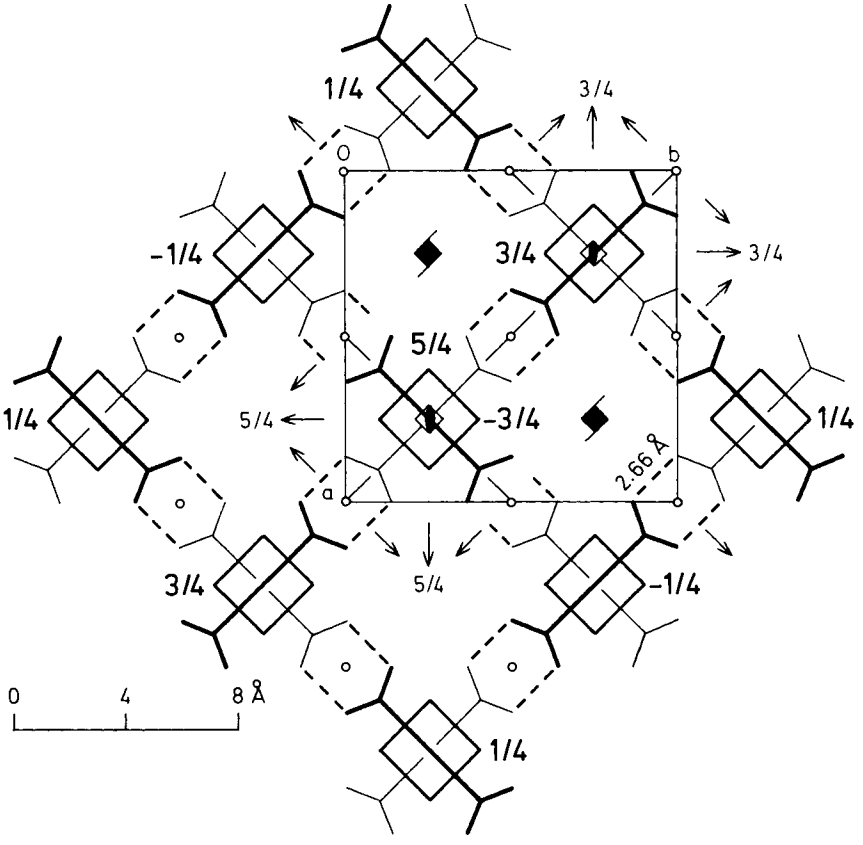

Fig. 2. *Space-group symmetry diagram of* **4**·*(MP-DMH-M), projected along the tetragonal* c *axis.* The symmetry elements of the space group $P4_2/nnm$ are shown, except glide planes and twofold screw axes; the unit cell origin coincides with a center of symmetry. Elevations of the molecular centers at D_{2d} sites are given in units of *c*. Ten molecules of the host **4** are drawn, which set up a H-bonded super-adamantane framework (2 central molecules superimposed, see also *Fig. 3*); the guest molecules are disordered and could not be localized in the X-ray analysis. The C=C bonds extending to the *exo*-methylidene groups of **4** are oriented along the *c* axis and are thus not visible in this projection. The pairwise H-bonds between the COOH groups are indicated by dashed lines and their O(H)O distance is included.

inner reflections, and unit weights led to $R = 0.250$ and three residual density maxima of 2.14, 1.49, and 1.17 e $Å^{-3}$, located on special positions in the cavities between the tetra-acid host molecules; all results on **4**·(MP-DMH-M) reported here are based on the refinement excluding the inner reflections as detailed in *Table 1*. The final atomic coordinates and temperature-factor coefficients of **4**·(MP-DMH-M) are listed in *Table 2*, while *Fig. 1* shows the termal ellipsoids, some selected structural data, and the atomic numbering. A space-group symmetry diagram appears in *Fig. 2*, and *Fig. 3* illustrates various aspects of the double-diamond host architecture of **4**·(MP-DMH-M). Finally, *Figs. 4* and *5* highlight the closely analogous double-diamond structures of the α-tetragonal boron allotrope T-50 and of cuprite Cu_2O, respectively.

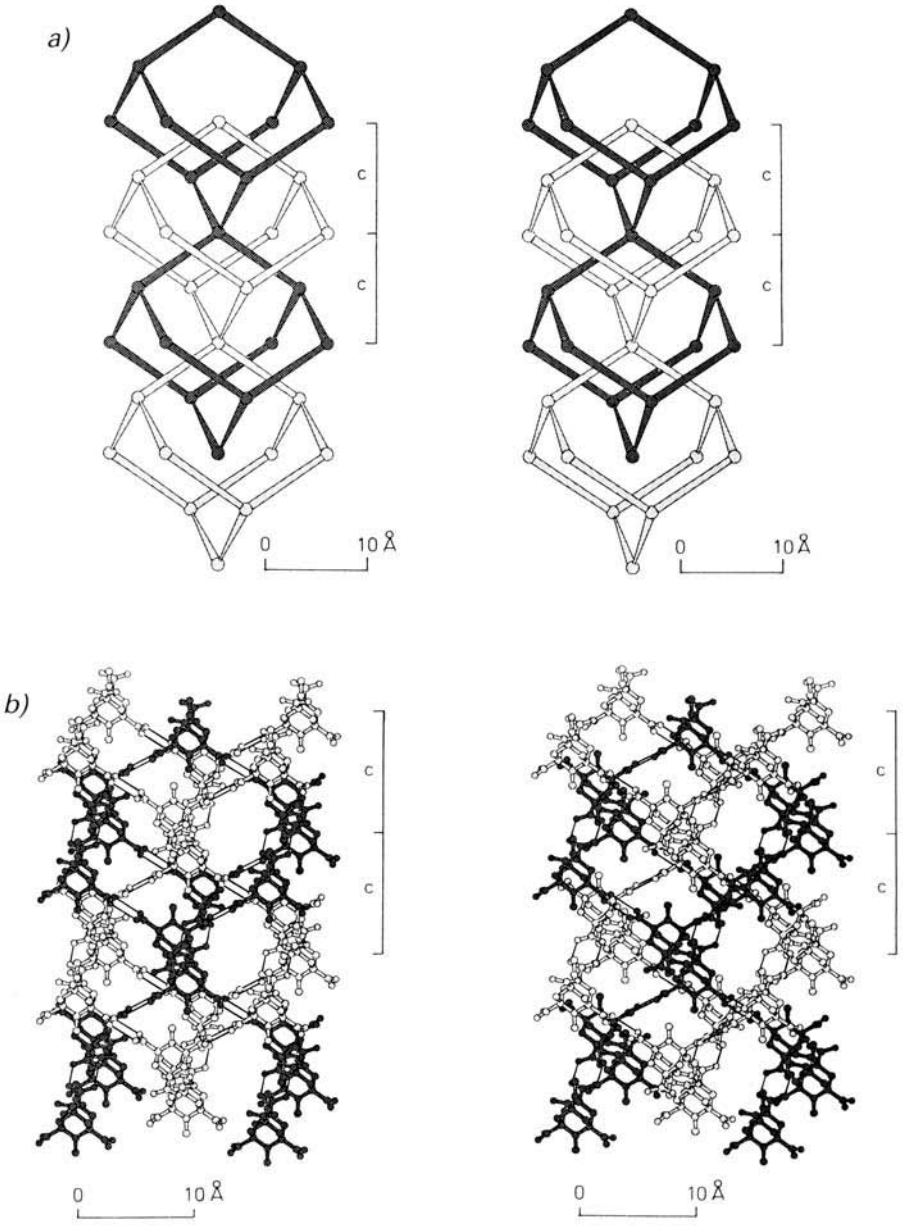

Fig. 3. *Double-diamond-like host architecture of* **4**·(MP-DMH-M) . a) *Diagrammatic stereoview* (*c* axis vertical) *of the two interpenetrating super-diamond networks* (dark and light grey, resp.) *represented by two connected super-adamantane units*. The spheres represent the tetrahedral dimethylideneadamantane cores at their centers (D_{2d} sites), while the interconnecting rods symbolize the COOH groups linked by pairwise H-bonds (see *Fig. 2*). b) *Ball-and-stick representation of the two interpenetrating super-diamond networks* (*c* axis approximately vertical, H-atoms omitted). A H-bonded super-adamantane unit and some additional elements of each network are shown. Note that the C=C bonds joining the *exo*-methylidene groups and the adamantane cores are directed along the tetragonal *c* axis.

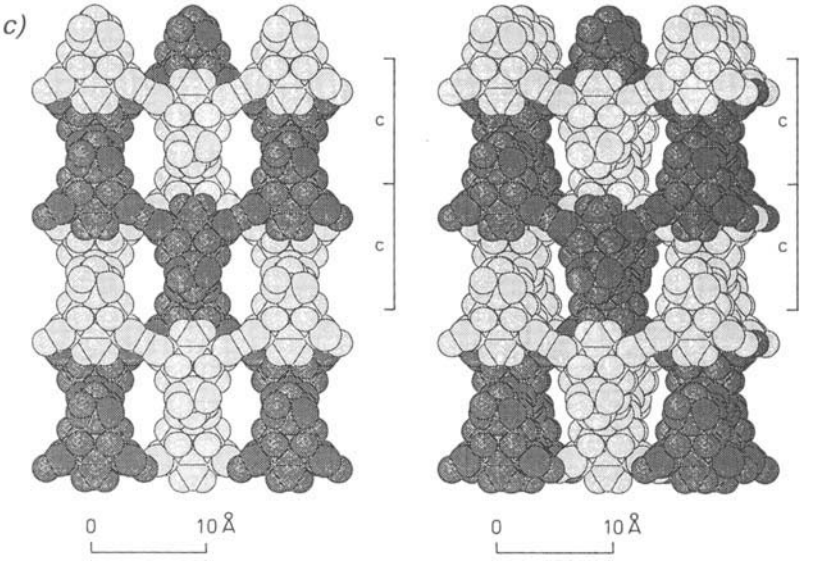

Fig. 3 (*cont.*). c) *Space-filling stereoview similar to* Fig. 3b (along bisector between *a* and *b* axes for left member of pair, *c* axis vertical). The cavities are occupied by the guest species **5**, **6**, and **7**, which are disordered and could not be 'seen' in the electron-density maps. Note that the two interpenetrating super-diamond networks have no *van-der-Waals* contacts.

Inclusion Compound of **4** *with Mesitylene* (**7**) (**4**·M_2). This complex was crystallized in the same way as **4**·(MP-DMH-M), except that a maximum amount of **7** was added to the acetone solution of **4**·H_2O without precipitating the tetra-acid (**4** is insoluble in pure mesitylene). Furthermore, a beaker with mesitylene was placed in the desiccator, in order to offer an excess of guest material as large as possible to the tetra-acid host. Clear octahedral crystals of **4**·M_2 appeared within *ca.* 1 week. They are sensitive to moisture, yet virtually indefinitely stable under mesitylene. For the intensity measurements, a crystal was mounted in a capillary together with a drop of mesitylene. Composition and stoichiometry of **4**·M_2 were analyzed by ^{1}H-NMR and density measurements. The spectra indicated a certain loss of *ca.* 5% mesitylene relative to the ideal ratio **4**/**7** = 1:2, yet this was neglected further on, and all crystallographic calculations were performed assuming the 1:2 ratio. It is also noted that the ^{1}H-NMR data suggested the crystals of **4**·M_2 to be contaminated by a small amount (less than 2%) of the half-olefinated 2-oxo-6-methylideneadamantane-1,3,5,7-tetracarboxylic acid. Crystallographic symmetry of tetra-acid host molecules of **4**·M_2 is D_2, of mesitylene guest species C_2 (twofold orientational disorder of Me groups on C_2 axis); *E*-map based on direct-method phases showed all host and guest heavy atoms, except for the mesitylene Me C-atom on the twofold axis, which was located subsequently by difference *Fourier* synthesis; refinement of the atomic parameters of **4**·M_2 as follows: C,O-atoms of host and guest anisotropic, H-atoms of host isotropic, H-atom positions of guest calculated and fixed. The final refined atomic parameters of **4**·M_2 are collected in *Table 3*. Thermal ellipsoids, selected geometry data, and the atomic numbering are shown in *Fig. 6*. A space-group symmetry diagram is drawn in *Fig. 7*, and *Fig. 8* shows various stereoviews of the

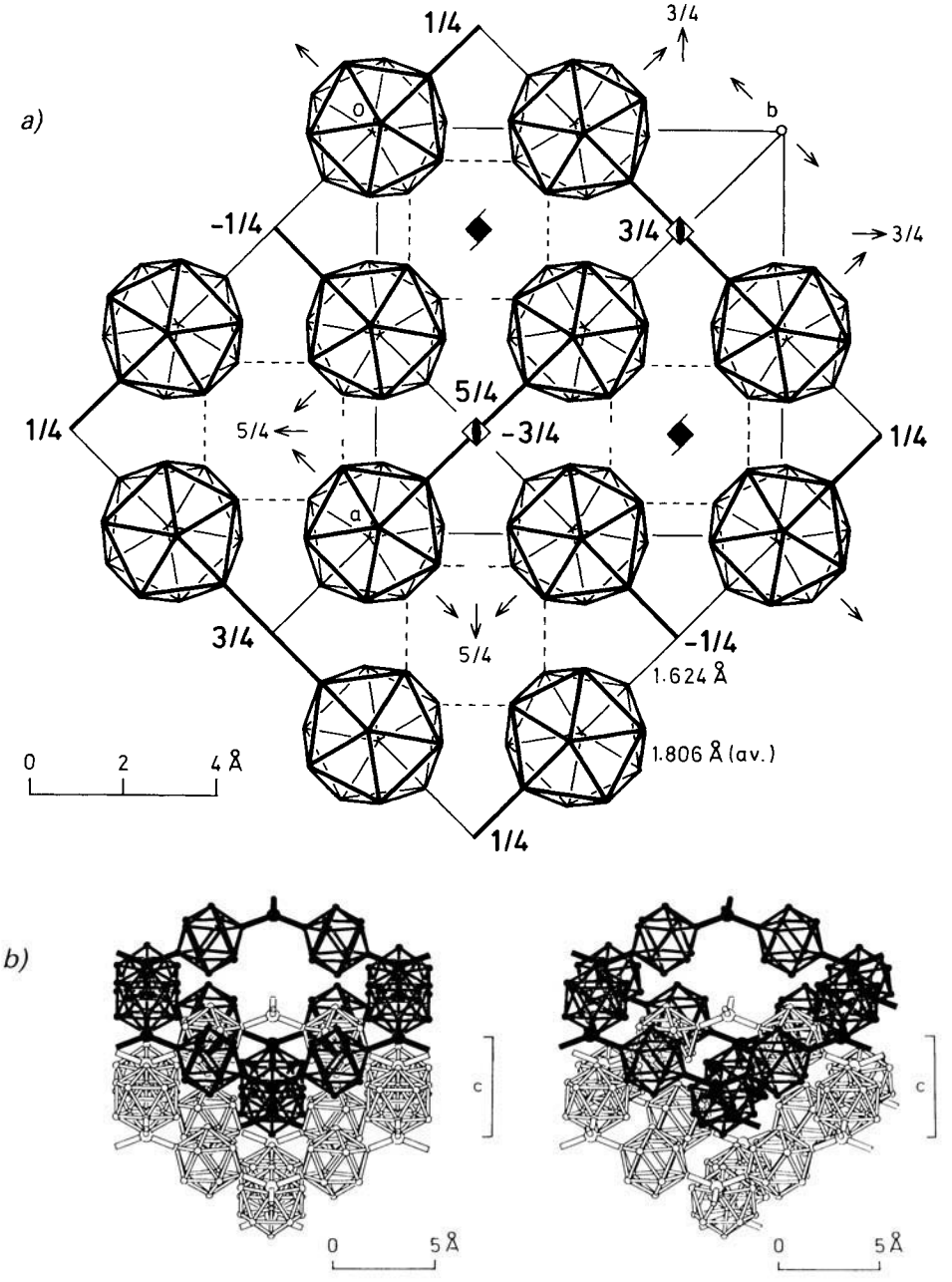

Fig. 4. *Double-diamond-like nature of the crystal structure of α-tetragonal boron* [T-50 boron, $B(B_{12})_2$]. a) *Space-group symmetry diagram* (to be compared to *Fig. 2* with same representation). A super-adamantane unit is shown, which is formed by 10 (tetragonally compressed) tetrahedral B-atoms and 12 B_{12} icosahedra. Additional intradiamond-like B–B bonds arranged in helices around the 4_2 screw axes are shown as dashed lines. Interdiamond-like B–B bonds cross-linking the two interpenetrating super-diamond networks are omitted; note that in the complete structure every icosahedral B-atom is bonded to 6 partners. Lengths of the intraicosahedral bonds (average) and

Table 3. *Refined Atomic Coordinates* ($\times 10^4$, hydrogen $\times 10^3$) *and Temperature Parameters* ($\times 10^3$) *of* **4**·M_2. See *Figs. 6c, d* for atomic numbering (H_{ox}: COOH H-atom) and compare legend of *Table 2* for more details.

	x	y	z	U_{11}	U_{22}	U_{33}	U_{23}	U_{13}	U_{12}
C(1)	3(2)	1722(1)	870(1)	25(1)	23(1)	21(1)	0(1)	−2(1)	−3(1)
C(2)	−767(2)	= 1/4 + x	1250	27(2)	= U_{11}	24(2)	5(1)	= −U_{23}	−1(2)
C(3)	783(2)	= 1/4 − x	1250	27(2)	= U_{11}	27(2)	−3(1)	= U_{23}	4(2)
C(4)	0	2500	501(2)	31(2)	25(2)	21(2)	0	0	−1(2)
C(5)	−1336(2)	= 1/4 + x	1250	44(2)	= U_{11}	52(3)	−11(2)	= −U_{23}	−13(2)
C(6)	0(2)	959(2)	489(1)	36(2)	23(2)	29(1)	−2(1)	1(2)	−2(2)
O(1)	380(2)	328(1)	659(1)	96(2)	28(1)	49(2)	−10(1)	−28(1)	18(1)
O(2)	−357(2)	988(1)	23(1)	100(2)	40(1)	42(1)	−16(1)	−39(1)	13(1)
H(3)	127(1)	165(1)	100(1)	25(7)					
H(4)	43(1)	249(2)	27(1)	20(6)					
H(5)	−176(2)	119(2)	149(1)	42(8)					
H_{ox}	29(2)	−13(3)	38(2)	133(16)					
CM(1)	2500	961(4)	0	62(4)	49(4)	120(6)	0	−23(4)	0
CM(2)	2983(3)	1393(3)	386(2)	55(3)	66(3)	89(3)	10(3)	−14(2)	−6(2)
CM(3)	2975(2)	2245(2)	392(2)	58(3)	61(3)	53(2)	−2(2)	19(2)	−18(2)
CM(4)	2500	2651(3)	0	81(4)	48(4)	56(3)	0	21(4)	0
CM(5)	2500	28(5)	0	114(6)	48(4)	230(10)	0	−85(7)	0
CM(6)	3506(3)	2702(3)	815(2)	102(4)	97(4)	59(2)	−15(3)	19(3)	−39(3)
HM(2)	334	108	66	67(9)					
HM(4)	250	327	0	67(9)					
HM(5A)	212	−18	−30	162(11)					
HM(5B)	231	−18	38	162(11)					
HM(5C)	307	−18	−7	162(11)					
HM(6A)	343	331	76	162(11)					
HM(6B)	410	256	75	162(11)					
HM(6C)	334	254	121	162(11)					

double-diamond-like host-guest architecture of **4**·M_2. Finally, three known structures, which may be related to **4**·M_2 and also crystallize in space group $I4_1/acd$, are illustrated in *Fig. 9* for comparison.

Inclusion Compound of **4** *with* **5** *and* **7** (**4**·(MP-M)). This complex, whose crystallography is closely similar to that of **4**·M_2, was crystallized in the same fashion as **4**·(MP-DMH-M) by dissolving **4**·H_2O in acetone and removing the solvent with P_2O_5 in a desiccator. In the majority of cases, this procedure furnished crystals of **4**·(MP-DMH-M) (see above), while more or less accidentally a few truncated octahedral specimen were identified as **4**·(MP-M). Composition and stoichiometry of **4**·(MP-M) were again analyzed by ^{1}H-NMR (**4**/**5**/**7** = 1:0.4:1.6). The macroscopic crystal behavior of **4**·(MP-M), **4**·M_2, and **4**·(MP-DMH-M) is very similar, and the crystallographic measurements of the three complexes proceeded more or less in the same way. Crystallographic symmetry

the extraicosahedral bonds between hexa- and tetravalent B-atoms are given. b) *Stereoview of the double-diamond-like architecture*. The ball-and-stick diagram shows two concatenated super-adamantane frameworks representing the two interpenetrating super-diamond lattices. Additional intra- or interdiamond-like B–B bonds are not included. For clarity, the tetrahedral B-atoms are drawn with enlarged size. The pronounced tetragonal compression of both the tetrahedral B coordination and the super-diamond networks is clearly evident. The drawings are based on the atomic coordinates of [3].

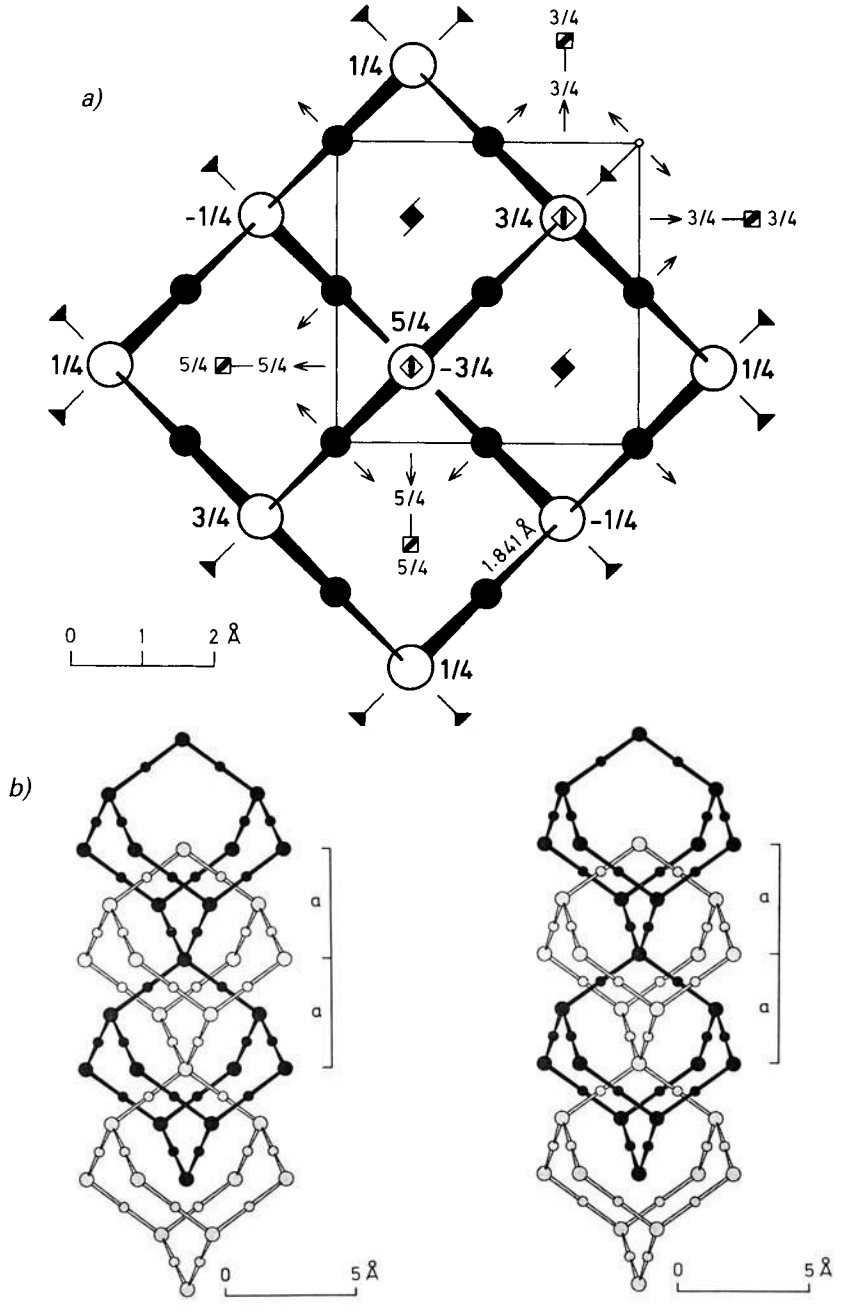

Fig. 5. *Double-diamond architecture of cuprite, OCu_2.* a) *Space-group symmetry diagram.* Large, tetrahedral centers: O (on T_d sites), small, linear centers: Cu (on D_{3d} sites). b) *Stereoview of the two interpenetrating, undistorted* (cubic) *super-diamond frameworks represented by two connected super-adamantane units.* Note that essentially the same double-diamond structure is taken up by $Zn(CN)_2$ and $Cd(CN)_2$ (replacement of O by Zn and Cd, resp., of Cu by CN).

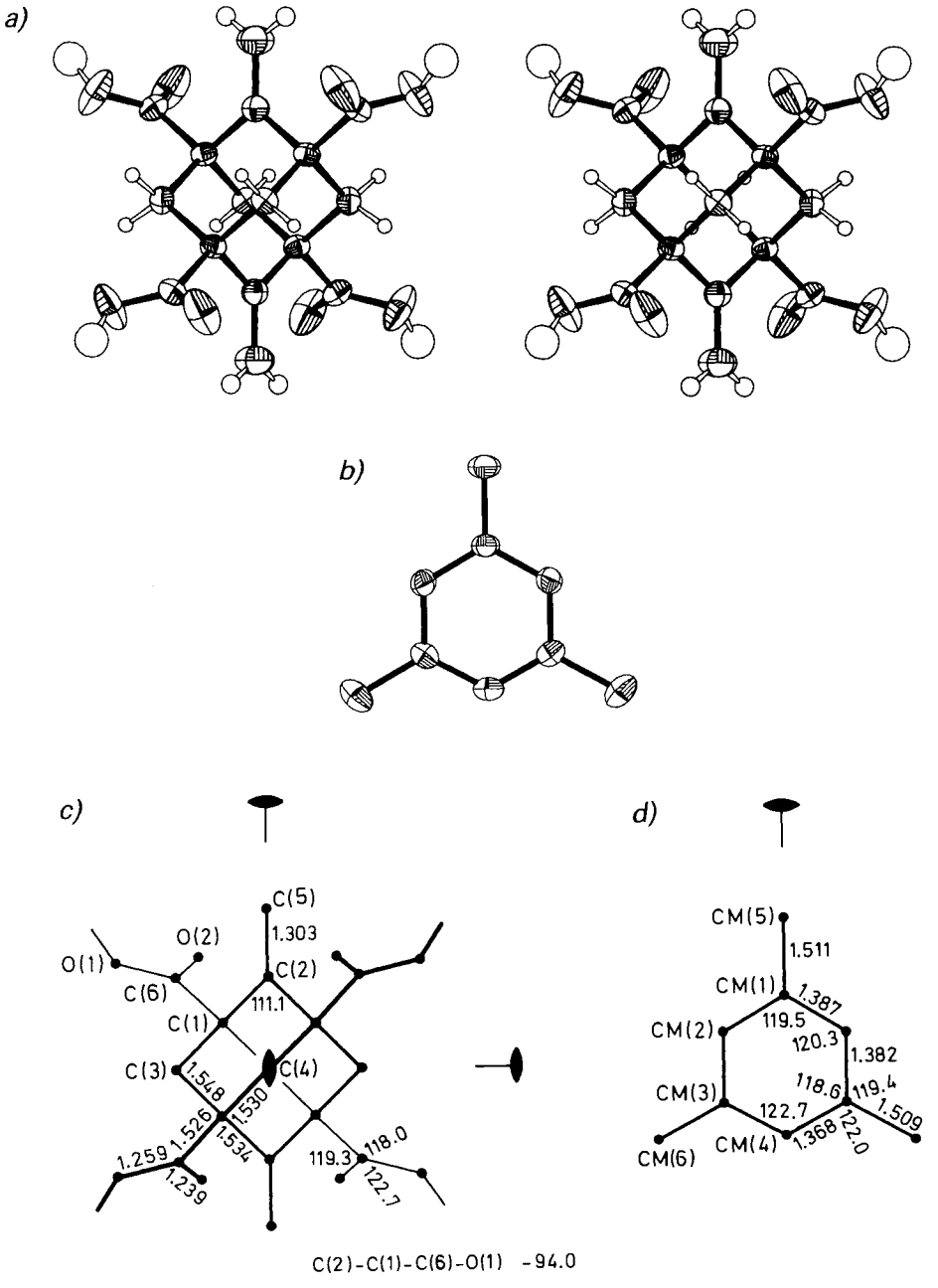

Fig. 6. *Crystal structure of* **4**·M_2 (crystallographic molecular symmetry of host **4**, D_2, of mesitylene guest, C_2). a) *Stereoview of* **4** (along a C_2 axis for right member of pair) *with vibrational ellipsoids* (50% probability, U_{iso} of H-atoms divided by 3). b) *Vibrational ellipsoids of mesitylene guest* (20%, H-atoms omitted). c) d) *Atomic numbering and selected geometry data* (bond lengths [Å], bond angles, and torsion angle [°]); estimated average standard deviations *ca.* 0.005 Å and 0.3° for **4**, 0.008 Å and 0.5° for mesitylene.

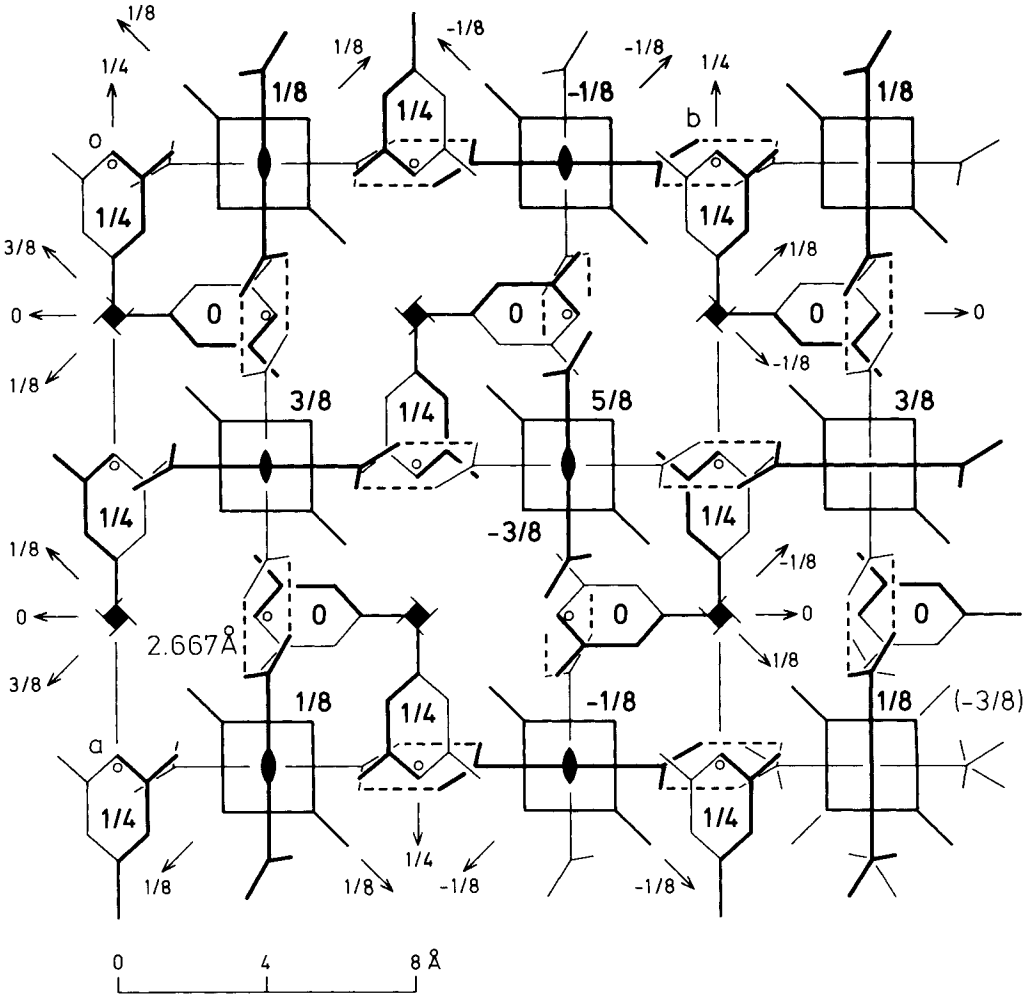

Fig. 7. *Space-group symmetry ($I4_1/acd$) diagram of* **4**·M_2, *projected along tetragonal* c *axis.* S_4 axes, glide planes, and 2_1 screw axes not shown, origin on center of symmetry. The representation is similar to that of *Fig. 2* (see corresponding legend for more details) applying to **4**·(MP-DMH-M). Note that in **4**·M_2 the exocyclic C=C bonds ar perpendicular to the *c* axis. An additional tetra-acid molecule of the second interpenetrating super-diamond network is drawn in light lines (lower-right corner) in order to point out the non-translational equivalence and the orthogonality of the C=C bonds of the two networks. Note also that thc chains of guest molecules running along the *a* and *b* axes, resp., are antiparallel.

of tetra-acid host of **4**·(MP-M) is D_2, of mesitylene guest model (see below) C_2; direct methods clearly furnished the locations of the host heavy atoms, yet not those of the guest atoms; subsequent *Fourier* synthesis based on host phases produced the C_2-symmetric mesitylene guest structure, which assumed anomalous geometrical features and both high and unusual thermal motion characteristics in the following refinement; mesitylene

structure is in fact merely a refinement *model* accounting for an *average* electron density of partially disordered M *and* MP guest molecules; anomalies of averaged mesitylene model may be rationalized in terms of appropriate superposition construct of the two different guest species (see *Discussion*); mesitylene guest model of **4**·(MP-M) refined with full weight (as in **4**·M_2), corresponding to cell content of 8 molecules of host **4** and 16 molecules of **7**; refinement of the complex **4**·(MP-M) under following conditions: C,O-atoms of host **4** and mesitylene guest model anisotropic, H-atoms of host isotropic, H-atoms of guest model not considered. *Table 4* lists the refined atomic parameters of **4**·(MP-M), and *Fig. 10* shows thermal ellipsoids, selected structural data, and atomic numbering as well as diagrams interpreting the partial guest disorder in terms of the superposition model referred to above and in the discussion.

Inclusion Compound of **4** *with (*tert*-Butyl)benzene* **8** (**4**·TBB). Crystallization of this complex proceeded similarly as for **4**·M_2 by dissolving **4**·H_2O in a mixture of acetone and (*tert*-butyl)benzene (**8**), and removal of the former with P_2O_5 in a desiccator vapor-saturated with **8**. The resulting moisture-sensitive lozenges were mounted in glass capillaries, together with a droplet of **8**. ^{1}H-NMR analysis gave a non-stoichiometric composition **4**/**8** of 1:1.7. Space group of **4**·TBB is $F2/d$ or Fd (corresponding standard space groups $C2/c$ and Cc, resp., see *Discussion* for reasons of non-standard choice of space group, centrosymmetry assumed); equivalent positions of $F2/d$: (0,0,0; 0,1/2,1/2; 1/2,0,1/2; 1/2,1/2,0) + (x,y,z; $1/4-x,y,1/4-z$; $-x,-y,-z$; $1/4+x,-y,1/4+z$); no crystallographic symmetry imposed on tetra-acid molecules; a sensible structural model could be delineated by direct methods for the tetra-acid host, yet not for the (*tert*-butyl)benzene guest, which is evidently highly disordered; only the host structure of **4**·TBB could thus be refined (C,O anisotropic, H-coordinates calculated and fixed, H-atoms of twofold orientationally disordered COOH groups not considered); 802 inner reflections with $\sin\Theta < 0.23$ excluded from refinement (*Table 1*); $R = 0.196$ for all 3474 reflections with $F_0 > 4\sigma(F_0)$, including inner reflections. *Table 5* lists the refined atomic parameters of the host tetra-acid of **4**·TBB, and *Fig. 11* depicts thermal ellipsoids, some selected structural data, and the atomic numbering. *Fig. 12* shows a space-group symmetry diagram, and *Fig. 13* depicts various stereoviews of the asymmetric double-diamond host structure of **4**·TBB.

Further Inclusion Compounds of **4** *with Bulky Guest Molecules.* In further attempts to enforce a single super-diamond inclusion compound of **4**, a couple of potential guest molecules still bulkier than (*tert*-butyl)benzene were tried. Good crystals of an inclusion compound of **4** could be grown with (*tert*-butyl)cyclohexane as the sole guest (similar crystallization procedure as for **4**·M_2); molar host-guest ratio 1:1.0 from ^{1}H-NMR. These monoclinic crystals are similarly shaped as those of **4**·TBB and also have similar cell constants (F-centered non-standard cell): $a = 23.033(6)$, $b = 22.952(4)$, $c = 22.904(6)$ Å, $\beta = 91.77(2)^0$, $V = 12102$ Å^3; with 16 molecules of **4** + 16 molecules of (*tert*-butyl)cyclo-hexane, a density $d_x = 1.046$ g·cm^{-3} is obtained. From the comparatively high host-guest ratio and the close crystallographic similarities with **4**·TBB, it may be tentatively conlcuded that the space group of the (*tert*-butyl)cyclohexane complex of **4** is also $F2/d$, and that it involves an asymmetric double-diamond-like host architecture, too. No detailed X-ray analysis was performed, however.

Crystals of good X-ray quality could also be obtained by offering DL-α-pinene as guest molecules to **4**. Crystallization was performed as for **4**·M_2 by removing the acetone

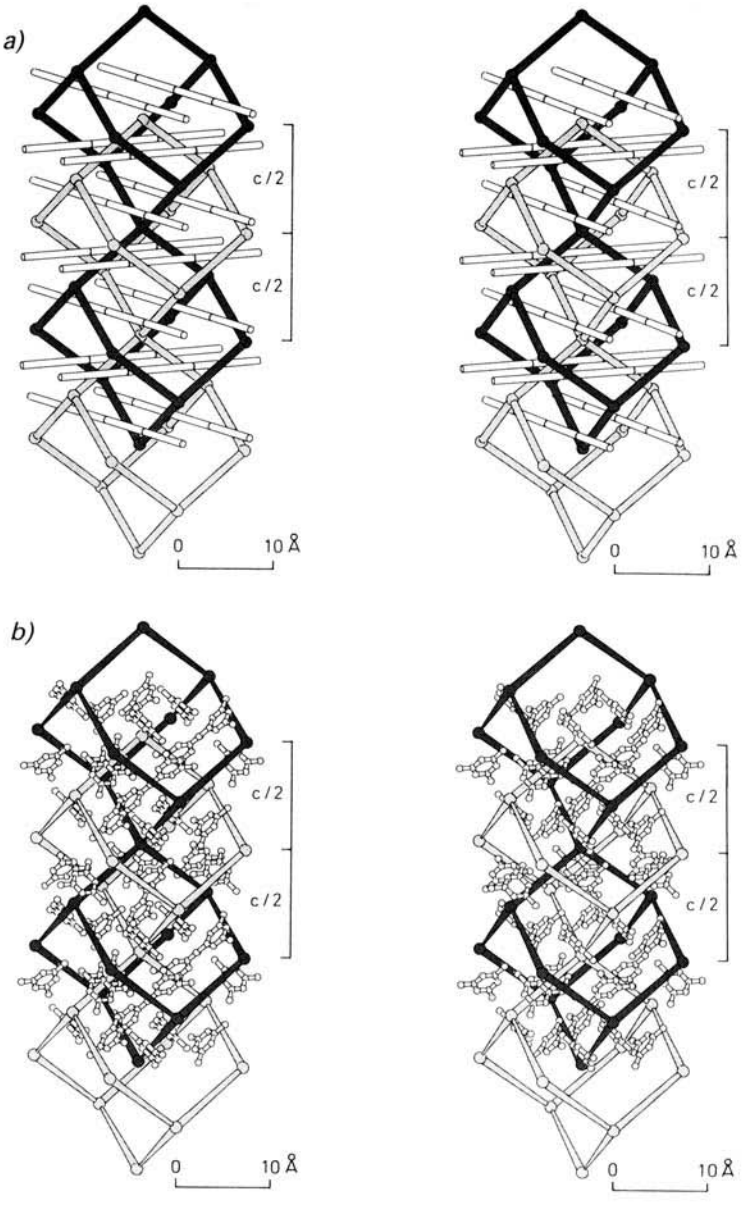

Fig. 8. *Host-guest architecture of* $\mathbf{4} \cdot M_2$. a) *Diagrammatic stereoview of the double-diamond-like host structure.* The representation is the same as in *Fig. 3* (see corresponding legend, tetra-acid molecules of $\mathbf{4} \cdot M_2$ on D_2 sites). In addition, the system of interpenetrating, mutually orthogonal twofold axes is shown (white rods), on which the guest molecules reside. b) *Same view as* Fig. 8a, *with the interpenetrating twofold axes replaced by the actual mesitylene guest molecules.*

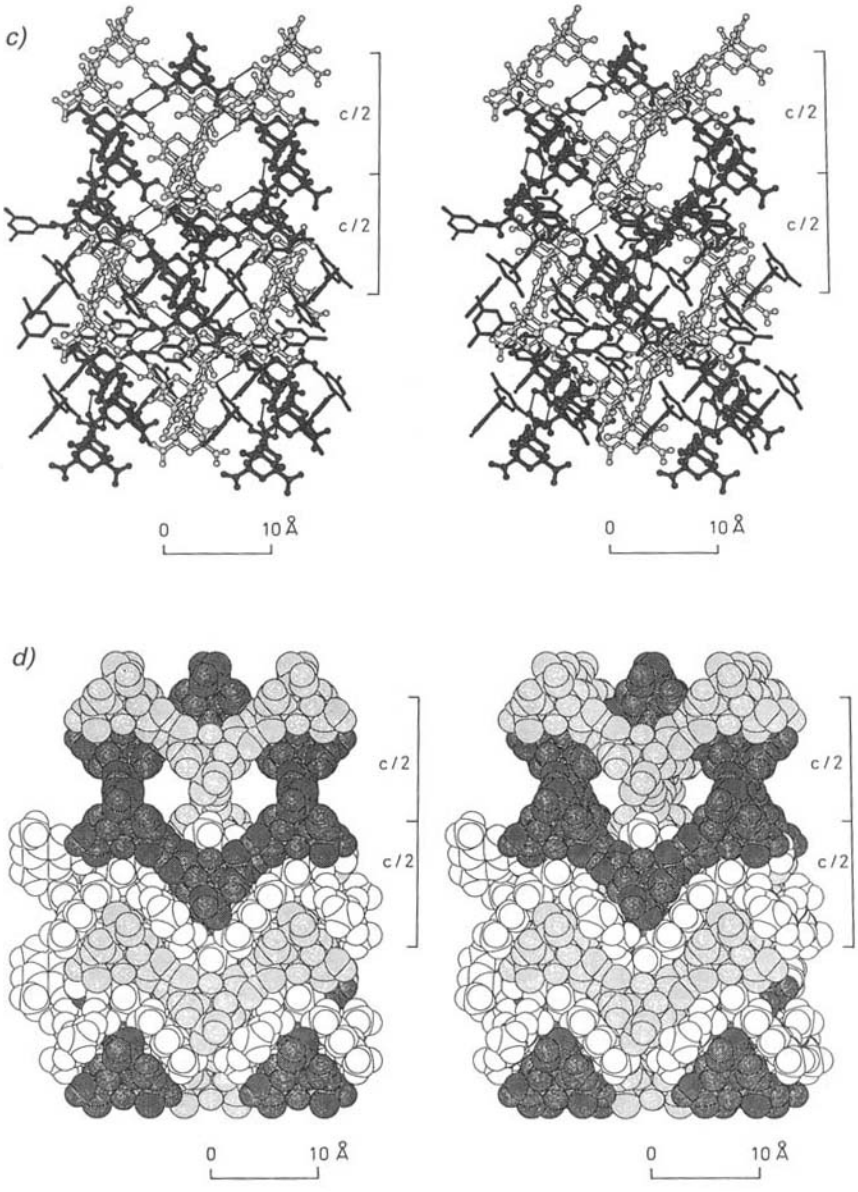

Fig. 8 (*cont.*). c) *Ball-and-stick stereorepresentation of complete host-guest architecture.* In the upper part of the drawing, the mesitylene guest molecules are removed in order to visualize the host cavities. d) *Similar view as* Fig. 8c *in space-filling representation.* For the left member of the stereopair, the view is along (respectively, perpendicular to) the twofold axes on which the mesitylene guest chains reside: visualization of the bottle-necks of the respective host channels in upper part of picture. The portions of the two superdiamond lattices shown in dark and light grey, respectively, comprise a super-adamantane unit plus 6 additional elements each; the mesitylene molecules are left white without shading. Note that the two super-diamond host lattices are not translationally equivalent, and that the mesitylene guest chains run antiparallel.

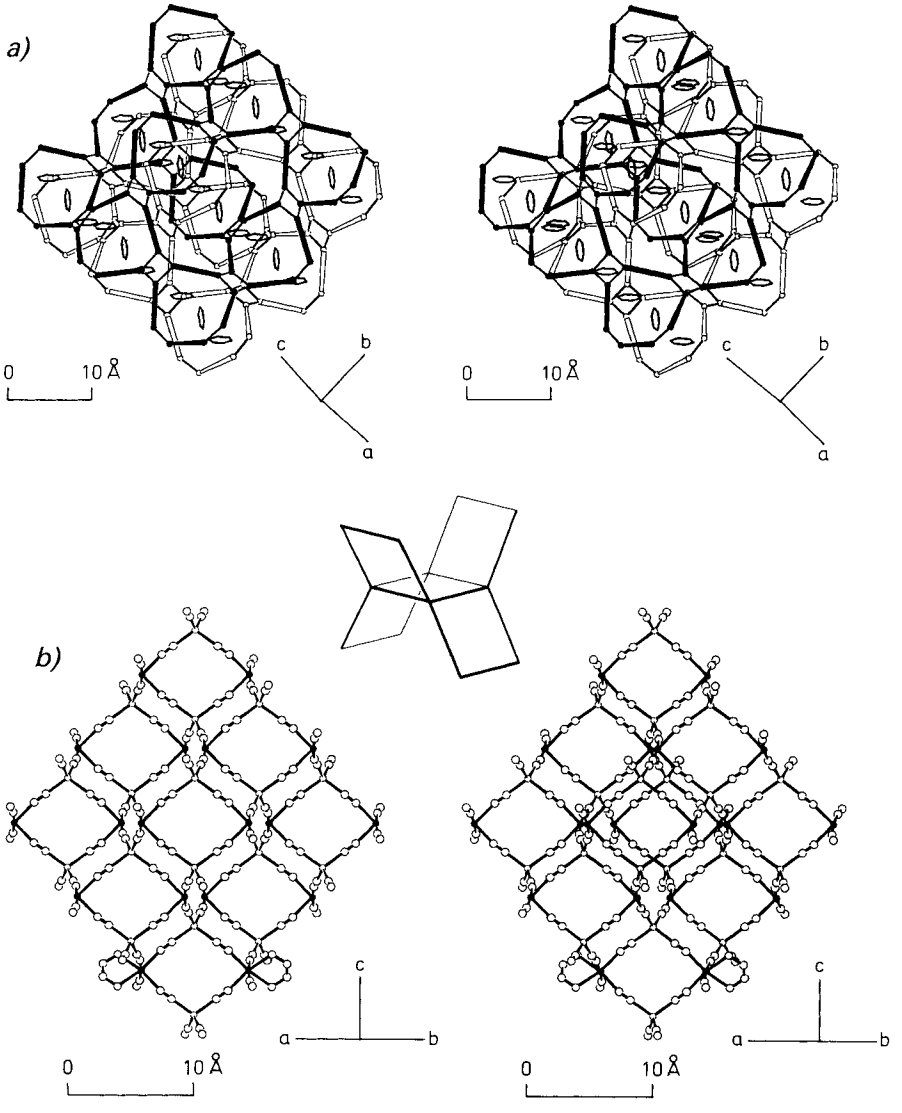

Fig. 9. *Stereoviews of three crystal structures related to* **4** · M_2 *with space group* $I4_1/acd$. a) *Double-diamond structure of an inclusion compound of a dimethylhomoadamantanediol with benzene guest molecules.* The drawing is based on the atomic coordinates of [4a]. Two symmetrically interpenetrating super-adamantane units (black and white, resp.) are shown diagrammatically as well as 9 chains of benzene guest molecules; the latter are partially disordered in the actual structure. The diol host molecules are represented by their O-atoms only, joined by thick rods, which stand for the hydrocarbon core. Thin lines connecting the O-atoms symbolize O(H)O H-bonds. The tetrahedral building blocks of the super-diamond networks consist of H-bonded cyclic diol tetramers; these tetramers are interlinked by pairwise additional H-bonds in tetrahedral fashion. The crystal axes shown indicate directions only. b) *Double-diamond structure of [Cd(en)Cd(CN)$_4$].* The drawing is based on atomic coordinates of [5]. *Top*: single super-adamantane unit; left member of pair projected along a (diagonal) twofold axis parallel to the bisector of the crystallographic *a* and *b* axes. The tetrahedral building blocks (sketched above) are made up of 4 Cd cations linked by CN anions in cyclic fashion. These $[Cd(CN)]_4$ rings (symmetry D_2) are held together by pairwise additional

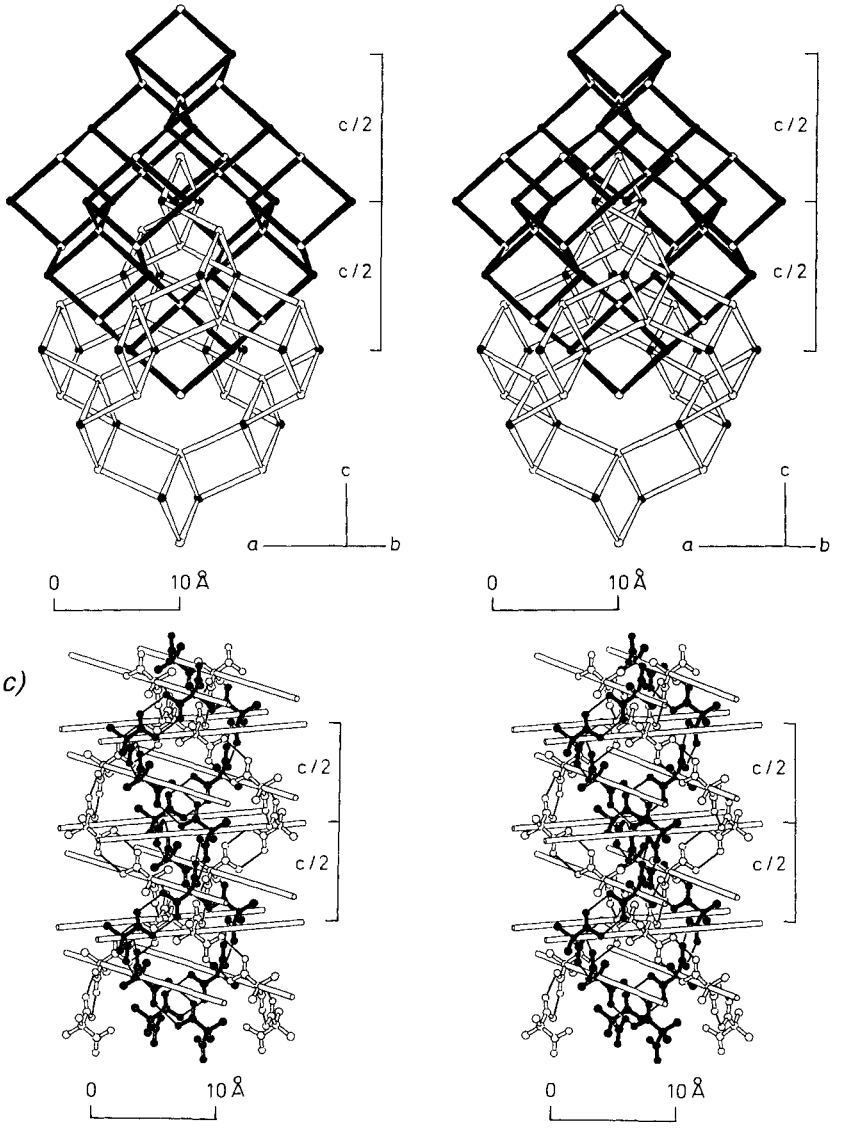

CN bridges in tetrahedral array. The cyanide linkages are thus seen to consist also of (a second type of) $[Cd(CN)]_4$ rings (symmetry C_i). The coordination of one half of the Cd ions is fourfold-tetrahedral (small open circles), of the other half sixfold-octahedral (small filled circles) due to an additional chelating ethylenediamine (en) ligand. Nothwithstanding the expanded complexation, the cyanide coordination of the octahedral Cd ions is still approximately tetrahedral. For clarity, the en ligands are drawn only for the two bottom Cd ions concerned. *Bottom*: diagrammatic view of two symmetrically interpenetrating super-diamond networks represented by super-adamantane units. Only the Cd ions are drawn; the interconnecting rods symbolize the cyanide bridges. The tetra- and hexa-coordinated Cd ions are distinguished as in the top drawing; the en ligands are not shown. The crystallographic axes shown again indicate directions only. c) *Dimethylmalonic acid, $C(CH_3)_2(COOH)_2$*. The drawing is based on atomic coordinates of [6]. Four helices of doubly H-bonded dicarboxylic-acid molecules are shown, which wind about 4_1 screw axes. The interpenetrating sets of thick white rods represent the twofold symmetry axes on which the diacid molecules reside; compare with Figs. *8a* and *b*.

Table 4. *Refined Atomic Coordinates* ($\times 10^4$, hydrogen $\times 10^3$) *and Temperature Parameters* ($\times 10^3$) of **4**·(MP-M). See *Fig. 10c, d* for atomic numbering (H_{ox}: COOH H-atom) and compare legend of *Table 2* for more details.

	x	y	z	U_{11}	U_{22}	U_{33}	U_{23}	U_{13}	U_{12}
C(1)	–4(3)	1718(2)	870(1)	32(2)	29(2)	28(2)	–2(2)	1(2)	–2(2)
C(2)	–769(3)	=1/4 + x	1250	32(2)	=U_{11}	29(4)	6(2)	=–U_{23}	–9(3)
C(3)	783(3)	=1/4 – x	1250	33(2)	=U_{11}	25(4)	–8(2)	=U_{23}	5(3)
C(4)	0	2500	498(2)	40(3)	24(3)	28(3)	0	0	1(4)
C(5)	–1327(4)	=1/4 + x	1250	51(3)	=U_{11}	62(5)	–13(3)	=–U_{23}	–15(4)
C(6)	2(3)	952(2)	490(2)	39(2)	32(2)	34(2)	–2(2)	–7(3)	–6(3)
O(1)	367(3)	312(2)	662(2)	103(3)	31(2)	62(3)	–9(2)	–35(2)	21(2)
O(2)	–359(3)	990(2)	26(2)	108(3)	43(2)	47(2)	–15(2)	–37(2)	13(2)
H(3)	129(3)	170(3)	100(2)	52(14)					
H(4)	45(2)	254(3)	25(1)	33(10)					
H(5)	–170(3)	122(4)	145(2)	55(18)					
H_{ox}	28(5)	–17(6)	30(4)	171(36)					
CMM(1)	2500	949(16)	0	103(13)	185(22)	268(26)	0	54(16)	0
CMM(2)	3016(8)	1312(11)	422(7)	139(12)	188(13)	267(18)	–70(14)	76(12)	–83(11)
CMM(3)	2985(7)	2190(12)	388(5)	113(9)	269(19)	111(8)	–25(11)	67(7)	–59(10)
CMM(4)	2500	2639(17)	0	118(13)	324(31)	99(11)	0	30(11)	0
CMM(5)	2500	–15(16)	0	187(18)	132(15)	415(36)	0	–71(22)	0
CMM(6)	3537(10)	2624(11)	824(6)	205(16)	305(20)	154(10)	–51(12)	52(10)	–103(15)

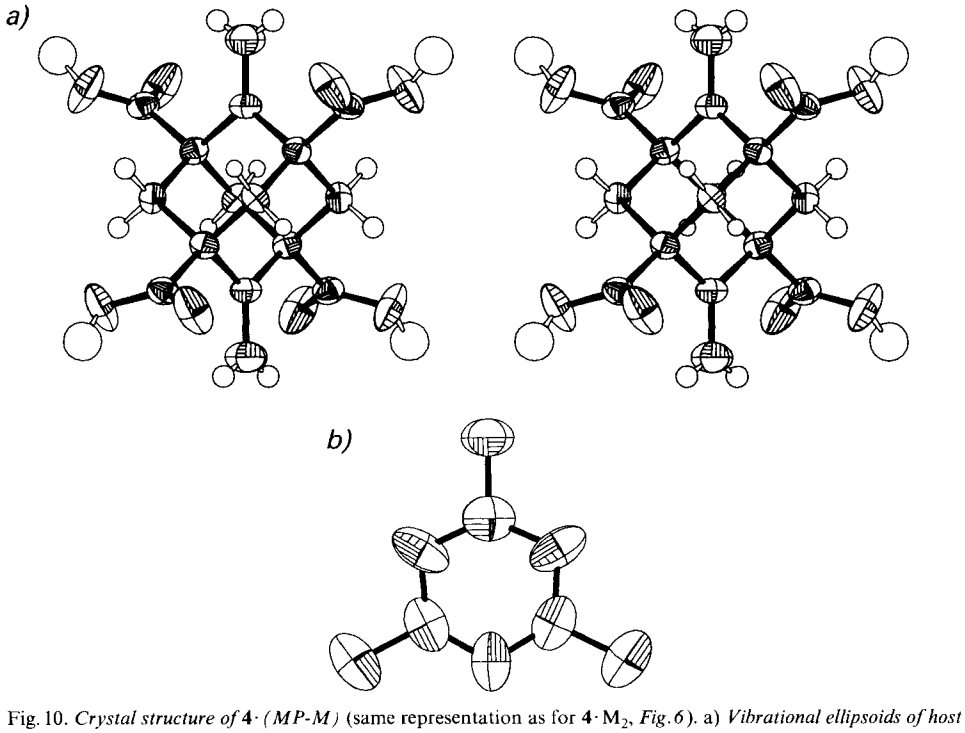

Fig. 10. *Crystal structure of* **4**·*(MP-M)* (same representation as for **4**·M_2, *Fig. 6*). a) *Vibrational ellipsoids of host tetra-acid* (50% probability, U_{iso} of H-atoms divided by 3). b) *Vibrational ellipsoids of guest mesitylene model* (20%, H-atoms omitted).

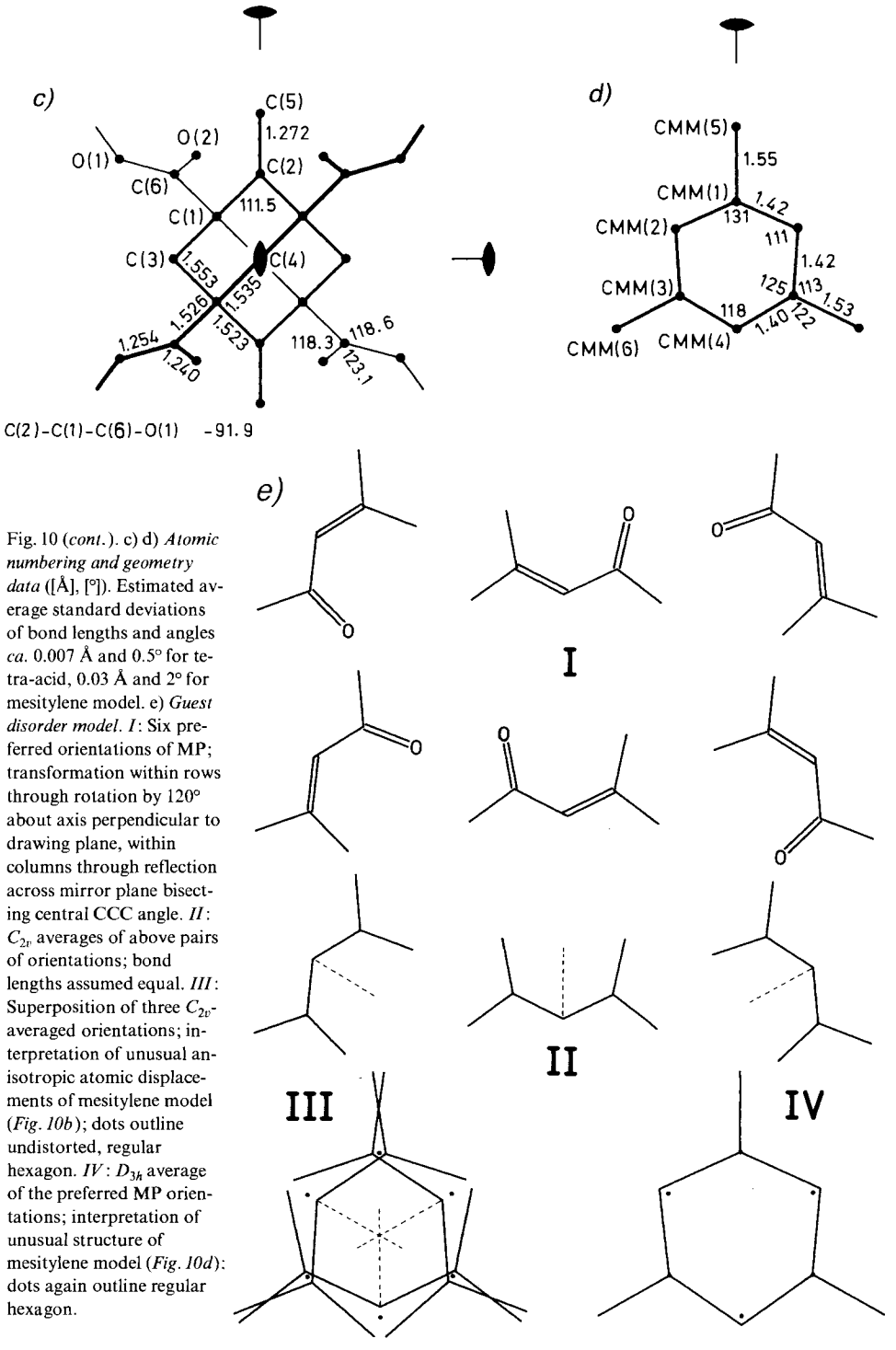

Fig. 10 (*cont.*). c) d) *Atomic numbering and geometry data* ([Å], [°]). Estimated average standard deviations of bond lengths and angles *ca.* 0.007 Å and 0.5° for tetra-acid, 0.03 Å and 2° for mesitylene model. e) *Guest disorder model. I*: Six preferred orientations of MP; transformation within rows through rotation by 120° about axis perpendicular to drawing plane, within columns through reflection across mirror plane bisecting central CCC angle. *II*: C_{2v} averages of above pairs of orientations; bond lengths assumed equal. *III*: Superposition of three C_{2v}-averaged orientations; interpretation of unusual anisotropic atomic displacements of mesitylene model (*Fig. 10b*); dots outline undistorted, regular hexagon. *IV*: D_{3h} average of the preferred MP orientations; interpretation of unusual structure of mesitylene model (*Fig. 10d*): dots again outline regular hexagon.

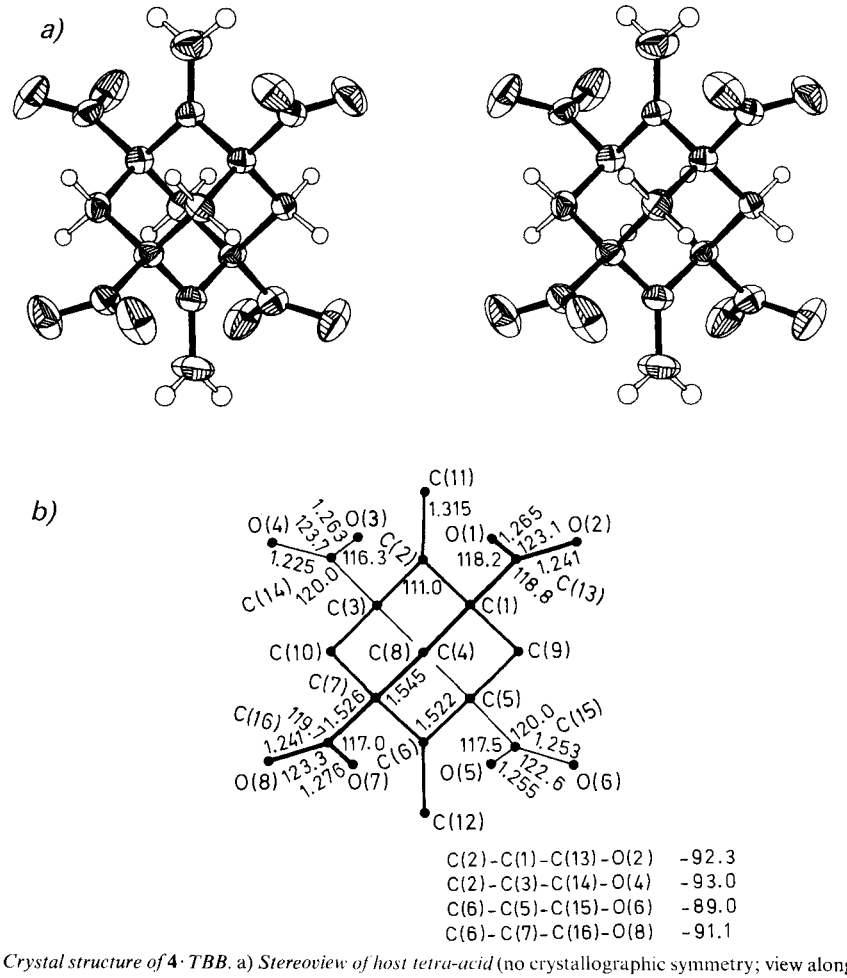

Fig. 11. *Crystal structure of* **4**·*TBB*. a) *Stereoview of host tetra-acid* (no crystallographic symmetry; view along axis C(8)/C(4) for right member of pair) *with vibrational ellipsoids* (50% probability, U_{iso} of H-atoms divided by 3). b) *Atomic numbering and selected bond lengths* [Å], *bond and torsion angles* [°]. Data of C-skeleton averaged over D_{2d} symmetry; estimated average standard deviations *ca.* 0.008 Å and 0.6°, resp. The TBB guest molecules are disordered.

solvent by P_2O_5 in a desiccator. However, ^{1}H-NMR analysis evidenced that the resulting crystals contained additional different guest molecules, which further experiments showed to originate from reactions (rearrangements?) of DL-α-pinene with P_2O_5 across the vapor phase. These crystals are again monoclinic with an *F*-centered cell very similar to that of **4**·TBB and the above inclusion compound of **4** with (*tert*-butyl)cyclohexane: $a = 23.175(9)$, $b = 22.834(5)$, $c = 22.845(9)$ Å, $\beta = 91.40(3)°$, $V = 12085$ Å^3, $d_m = 1.2$ g·cm^{-3} (CCl_4/DL-α-pinene, crude flotation experiment). Thus, rather likely the inclusion compound of **4** with DL-α-pinene plus products due to the action of P_2O_5 once again incorporates an asymmetric double-diamond-like host architecture (in accord with rough estimates of host-guest ratio). However, no detailed X-ray analysis was performed. It is

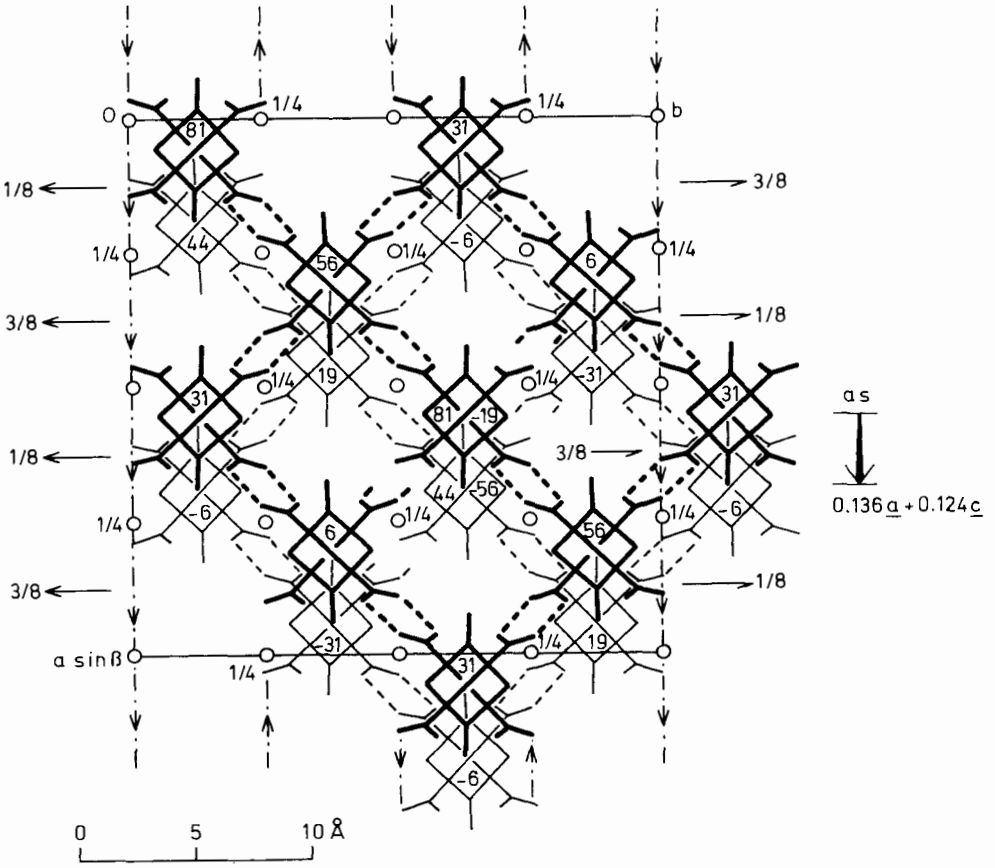

Fig. 12. *Space-group symmetry* ($F2/d$) *diagram of* **4**·*TBB*. A super-adamantane portion (plus an additional tetra-acid molecule) of both asymmetrically interpenetrating super-diamond networks is drawn (heavy and light lines, resp.; two central tetra-acid molecules superimposed). The elevations of the adamantane centers are given (units of $c/100$) and the asymmetry shift vector (as) is indicated. Note that the C=C bonds extending to the exocyclic methylidene groups are essentially all parallel and run approximately along the a axis.

noted that replacement of the racemic DL-α-pinene by optically active α-pinene or β-pinene in the above crystallizations did not yield useful crystals.

Several attempts to produce inclusion compounds of **4** with guests still more voluminous than (*tert*-butyl)cyclohexane or α-pinene appeared to be successful inasmuch presumable inclusion crystals precipitated, which, however, were of low grade as regards X-ray requirements. Hence, further details may de dispensed with. In conclusion, we have, therefore, so far not been able to unearth evidence supporting an inclusion compound of **4** with an extremely hollow H-bonded single super-diamond host architecture. Experimenting towards this goal is continuing in our laboratory with due consideration of the adamantane guest bulk limit pointed out in the *Discussion*, which should at least be exceeded, in order to break the double-diamond-like host structure of **4** in favor of a single-diamond-like architecture.

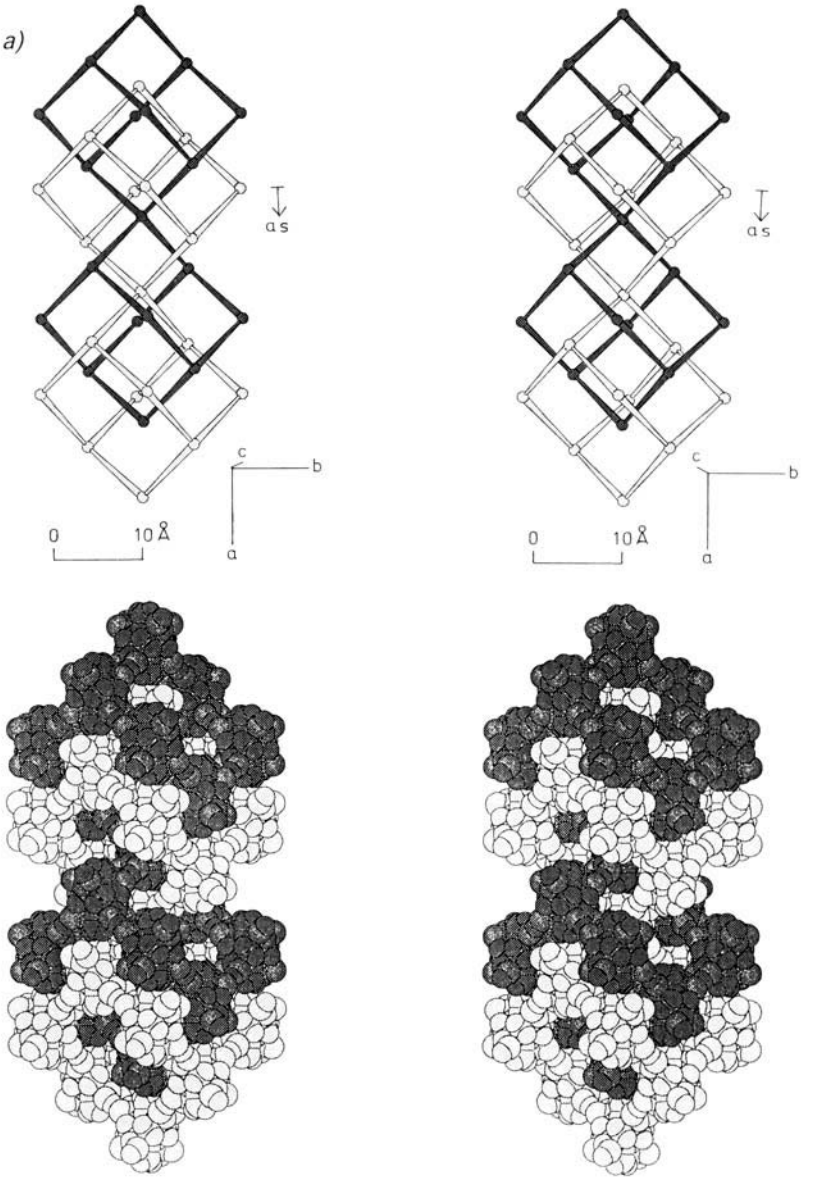

Fig. 13. *Asymmetric double-diamond-like host architecture of* **4** · *TBB.* The layout of the representations is similar to that of *Figs. 3* and *8*. Four different stereoviews of the two interpenetrating super-diamond networks (dark and light grey, resp.) are shown both in diagrammatic (*top*) and space-filling (*bottom*) notion (same scale throughout). The super-diamond networks are represented by two connected super-adamantane units cut out of these lattices. Spheres of diagrammatic views symbolize the dimethylideneadamantane cores of **4** at their centers, interconnecting rods the bridging, pairwise H-bonded COOH groups. The asymmetry shift vector (as) is shown as well as the crystallographic axes. The latter indicate directions only; the respective cell edge lengths are defined by the appropriate 'diagonals' (1,5 distances) of a super-adamantane unit. a) *View approximately along* c *axis.* Relationship with and generation out of triple-diamond structure of 2,6-dioxoadamantanetetracarboxylic acid (hydrate) as occuring in an inclusion compound with AcOH (see text).

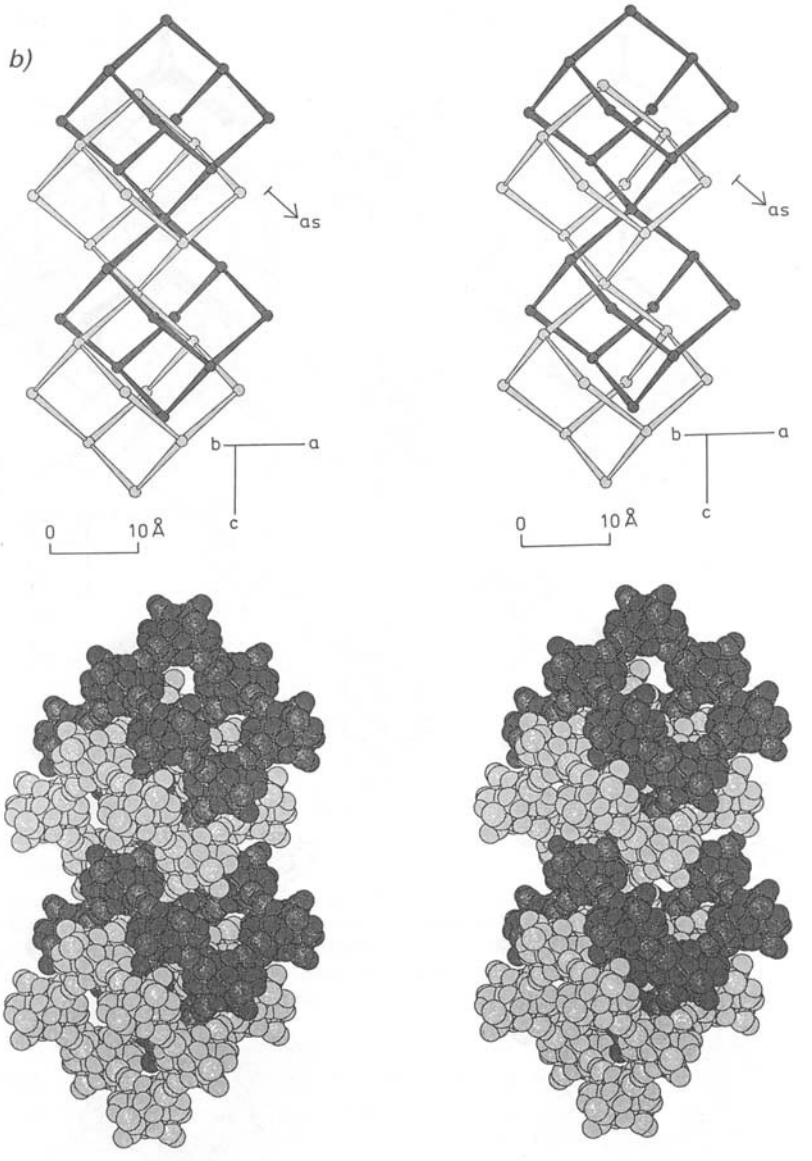

Fig. 13 (*cont.*). b) *View approximately along* b *axis showing the asymmetry shift vector* (as = 0.136**a** + 0.124**c**) *to run essentially parallel to the* a, c *bisector.*

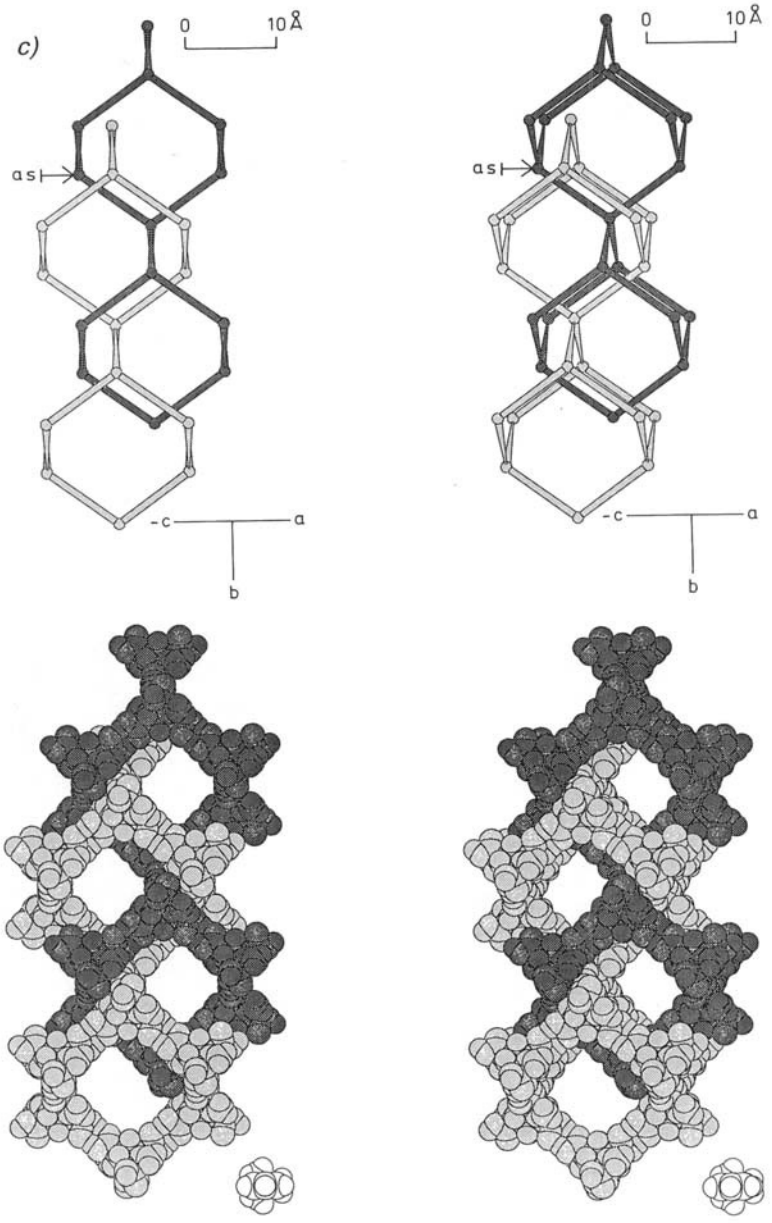

Fig. 13 (*cont.*). c) *View perpendicular to as vector and* b axis (for left member of stereoscopic pair). Visualization of the widened host channels as a consequence of the asymmetry shift. For comparison, a space-filling view of a **TBB** molecule (down long molecular axis, same scale) is shown below.

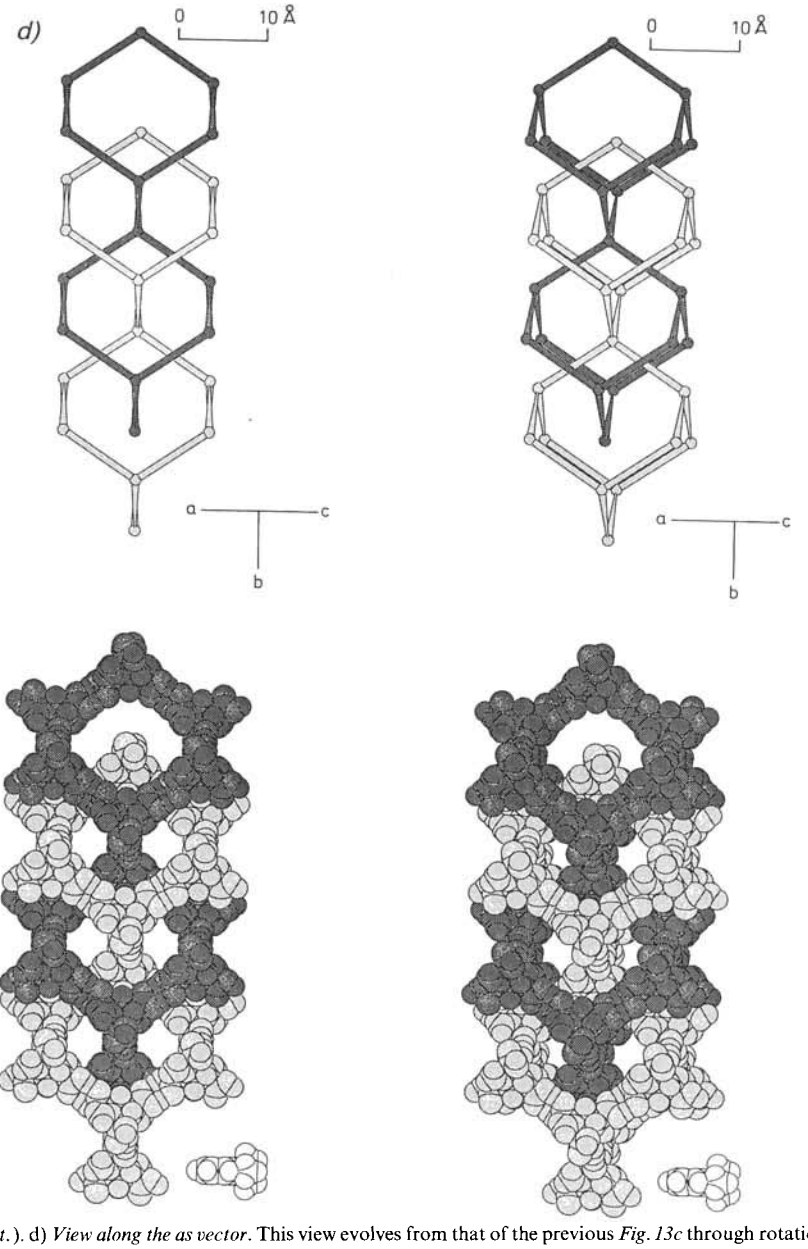

Fig. 13. (*cont.*). d) *View along the as vector*. This view evolves from that of the previous *Fig. 13c* through rotation by 90° about the *b* axis. It is provided to show the orthogonal channels unaffected by the asymmetry shift (compare with *Fig. 8d*). See text for more details.

Table 5. *Refined Atomic Coordinates* ($\times 10^4$, hydrogen $\times 10^3$) *and Temperature Parameters* ($\times 10^3$) of **4**·TBB. Guest molecules disordered; see *Fig. 11b* for atomic numbering and legend of *Table 2* for more details.

	x	y	z	U_{11}	U_{22}	U_{33}	U_{23}	U_{13}	U_{12}
C(1)	6544(2)	1652(2)	–244(2)	25(2)	32(3)	30(3)	0(2)	3(2)	0(2)
C(2)	6184(2)	1250(2)	–646(2)	26(3)	33(3)	29(3)	–1(2)	2(2)	–2(2)
C(3)	6565(2)	882(2)	–1032(2)	29(3)	32(3)	25(3)	–2(2)	1(2)	–1(2)
C(4)	6920(2)	1283(2)	–1413(2)	36(3)	33(3)	26(3)	–1(2)	–2(2)	–4(2)
C(5)	7304(2)	1682(2)	–1013(2)	24(2)	31(3)	29(3)	–6(2)	2(2)	–2(2)
C(6)	7677(2)	1310(2)	–611(3)	26(3)	38(3)	35(3)	–5(2)	2(2)	0(2)
C(7)	7328(2)	899(2)	–236(2)	27(3)	34(3)	31(3)	4(2)	–5(2)	1(2)
C(8)	6938(2)	1271(2)	158(2)	32(3)	36(3)	28(3)	2(2)	1(2)	5(2)
C(9)	6903(2)	2061(2)	–634(3)	28(2)	25(2)	32(2)	0(2)	3(2)	2(2)
C(10)	6959(3)	503(2)	–635(3)	35(2)	27(2)	33(2)	–5(2)	–1(2)	1(2)
C(11)	5628(3)	1239(4)	–660(4)	36(3)	71(5)	63(4)	–25(4)	–4(3)	–6(3)
C(12)	8240(3)	1338(3)	–591(3)	23(3)	69(4)	68(4)	11(4)	1(3)	3(3)
C(13)	6155(2)	2019(2)	141(2)	28(3)	34(3)	36(3)	1(2)	2(2)	2(2)
C(14)	6196(2)	479(3)	–1427(2)	29(3)	36(3)	36(3)	1(2)	–7(2)	–8(2)
C(15)	7667(2)	2075(3)	–1386(2)	34(3)	39(3)	29(3)	–5(2)	5(2)	–3(2)
C(16)	7715(2)	512(3)	148(2)	35(3)	37(3)	32(3)	–4(2)	–5(2)	5(2)
O(1)	5995(2)	1801(2)	622(2)	55(3)	68(3)	37(2)	4(2)	20(2)	14(2)
O(2)	6002(2)	2510(2)	–36(2)	57(3)	49(3)	69(3)	4(2)	26(2)	20(2)
O(3)	6014(2)	696(2)	–1908(2)	72(3)	55(3)	42(2)	4(2)	–26(2)	–24(2)
O(4)	6087(2)	–20(2)	–1265(2)	74(3)	43(3)	53(3)	10(2)	–27(2)	–28(2)
O(5)	7820(2)	1878(2)	–1874(2)	67(3)	56(3)	49(3)	–10(2)	30(2)	–24(2)
O(6)	7811(2)	2572(2)	–1201(2)	73(3)	42(3)	55(3)	–15(2)	29(2)	–26(2)
O(7)	7878(3)	719(3)	646(2)	86(4)	66(3)	51(3)	–14(3)	–38(3)	30(3)
O(8)	7869(2)	28(2)	–39(3)	71(3)	51(3)	66(3)	–11(2)	–29(2)	25(2)
H(4A)	667	153	–167	31(4)					
H(4B)	716	105	–168	31(4)					
H(8A)	671	101	42	31(4)					
H(8B)	717	152	43	31(4)					
H(9A)	713	234	–38	31(4)					
H(9B)	665	231	–89	31(4)					
H(10A)	720	25	–88	31(4)					
H(10B)	673	23	–39	31(4)					
H(11A)	541	97	–93	46(8)					
H(11B)	540	150	–40	46(8)					
H(12A)	847	108	–32	46(8)					
H(12B)	845	161	–85	46(8)					

Monohydrate of 2,6-Dimethylideneadamantane-1,3,5,7-tetracarboxylic Acid (**4**·H_2O). This very stable hydrate is only sparingly soluble in H_2O and was crystallized in a similar fashion as the parent adamantane-1,3,5,7-tetracarboxylic acid (**1**) [1] from an alkaline aqueous solution by gas-phase neutralization; note, however, that **1** crystallizes H_2O-free! The tetra-acid **4** was dissolved as carboxylate in aq. KOH and placed in a desiccator, together with a separate container of half-conc. HCl. Slow neutralization *via* the gas-phase yielded beautiful large crystals of distorted octahedral shape, which were mounted on a glass fibre. Two independent molecules each of **4** and H_2O without crystallographic symmetry; direct methods produced positions of all heavy atoms of **4**·H_2O without difficulty; subsequent refinement resulted in well-defined ordered structure of relatively low overall temperature motion; C- and O-atoms optimized anisotropically in the refinements, H-atoms isotropically. The refined atomic parameters of **4**·H_2O appear in *Table 6*,

Table 6. *Refined Atomic Coordinates and Temperature Parameters* ($\times 10^4$, hydrogen $\times 10^3$) of **4**·H_2O. See *Fig. 14b* for atomic numbering and legend of *Table 2* for more details.

	x	y	z	U_{11}	U_{22}	U_{33}	U_{23}	U_{13}	U_{12}
Molecules 1									
C(1)	2435(2)	4772(1)	6064(1)	203(6)	180(6)	174(6)	–7(5)	17(5)	56(5)
C(2)	3601(2)	4163(1)	6360(1)	184(6)	251(6)	176(7)	42(6)	45(5)	65(5)
C(3)	3226(2)	2741(1)	5947(1)	190(6)	232(6)	198(7)	51(5)	28(5)	93(5)
C(4)	1706(2)	1893(1)	6192(1)	203(6)	213(6)	224(7)	54(6)	33(6)	78(5)
C(5)	496(2)	2489(1)	5905(1)	179(6)	188(6)	202(7)	19(5)	28(5)	65(5)
C(6)	407(2)	2483(1)	4964(1)	238(6)	186(6)	200(7)	8(5)	22(6)	99(5)
C(7)	1905(2)	3305(1)	4702(1)	235(6)	204(6)	147(6)	8(5)	18(5)	92(5)
C(8)	2337(2)	4752(1)	5116(1)	233(6)	178(6)	182(7)	23(5)	19(6)	69(5)
C(9)	916(2)	3932(1)	6308(1)	196(6)	201(6)	192(7)	–9(6)	38(6)	68(5)
C(10)	3114(2)	2726(1)	4997(1)	227(6)	233(6)	192(7)	17(6)	51(5)	105(5)
C(11)	4721(2)	4758(2)	6933(1)	281(8)	361(8)	333(9)	4(7)	–67(7)	70(6)
C(12)	–803(2)	1873/2)	4449(1)	275(8)	364(8)	276(8)	20(7)	–36(7)	48(6)
C(13)	2874(2)	6218(2)	6453(1)	249(7)	211(6)	220(7)	–27(6)	–2(6)	55(5)
C(14)	4428(2)	2159(2)	6208(1)	225(6)	327(7)	232(7)	63(6)	49(6)	126(5)
C(15)	–1012(2)	1718(2)	6177(1)	193(6)	247(7)	252(7)	34(6)	13(6)	57(5)
C(16)	1820(2)	3325(2)	3765(1)	245(7)	248(7)	176(7)	4(6)	13(6)	74(5)
O(1)	3766(2)	7125(1)	6186(1)	468(7)	218(6)	450(7)	–45(5)	159(6)	–36(5)
O(2)	2179(1)	6358(1)	7108(1)	504(6)	225(5)	339(6)	–76(5)	165(5)	68(5)
O(3)	4270(1)	1289(1)	6647(1)	378(6)	520(6)	571(7)	326(5)	127(6)	267(4)
O(4)	5681(1)	2723(1)	5894(1)	317(5)	870(7)	829(8)	571(6)	279(6)	367(5)
O(5)	–1293(1)	438(1)	6164(1)	341(6)	235(5)	580(8)	50(6)	204(5)	20(5)
O(6)	–1865(1)	2258(1)	6417(1)	250(5)	409(6)	970(10)	145(7)	232(6)	157(4)
O(7)	1419(1)	4120(1)	3416(1)	638(6)	517(6)	204(5)	78(5)	9(5)	374(4)
O(8)	2249(2)	2397(1)	3380(1)	704(7)	371(5)	172(5)	25(5)	114(5)	302(4)
H(4A)	177(2)	189(1)	680(1)	19(4)					
H(4B)	145(2)	98(2)	594(1)	25(5)					
H(8A)	327(2)	525(2)	495(1)	27(5)					
H(8B)	159(2)	514(2)	495(1)	23(4)					
H(9A)	98(2)	392(2)	692(1)	32(4)					
H(9B)	14(2)	429(2)	614(1)	30(5)					
H(10A)	407(2)	325(1)	483(1)	19(4)					
H(10B)	287(2)	179(2)	474(1)	22(4)					
H(11A)	541(2)	433(2)	713(1)	37(5)					
H(11B)	489(2)	562(2)	719(1)	39(5)					
H(12A)	–173(2)	137(2)	464(1)	41(5)					
H(12B)	–84(2)	186(2)	385(1)	34(5)					
HO(2)	240(2)	718(2)	732(1)	46(6)					
HO(4)	638(3)	245(3)	607(2)	84(9)					
HO(5)	–216(2)	8(2)	633(1)	61(6)					
HO(8)	226(2)	249(2)	284(1)	58(6)					
OW	4049(1)	481(1)	3197(1)	275(5)	238(5)	320(6)	41(5)	–9(5)	59(4)
HW(1)	466(2)	119(2)	339(1)	62(8)					
HW(2)	452(3)	–10(2)	325(2)	75(8)					
Molecules 2									
C(1)	2130(2)	2646(1)	9193(1)	167(6)	217(6)	181(7)	27(5)	21(5)	73(5)
C(2)	1511(2)	1238(1)	8735(1)	202(6)	223(6)	157(6)	15(5)	36(5)	47(5)
C(3)	2491(2)	412(1)	8981(1)	214(6)	179(6)	175(7)	–12(5)	30(6)	45(5)
C(4)	4086(2)	1093(1)	8773(1)	228(6)	210(6)	214(7)	6(6)	65(6)	77(5)
C(5)	4720(2)	2507(1)	9238(1)	180(6)	187(6)	240(7)	17(6)	45(6)	63(5)
C(6)	4719(2)	2429(1)	10173(1)	224(6)	181(6)	242(7)	1(6)	0(6)	95(5)
C(7)	3145(2)	1743(1)	10395(1)	231(6)	197(6)	156(6)	–7(5)	10(5)	84(5)
C(8)	2153(2)	2551(1)	10132(1)	215(6)	214(6)	179(7)	–6(5)	27(5)	96(5)
C(9)	3725(2)	3321(1)	8975(1)	198(6)	200(6)	247(7)	55(6)	44(6)	71(5)

Table 6 (*cont.*)

	x	*y*	*z*	U_{11}	U_{22}	U_{33}	U_{23}	U_{13}	U_{12}
C(10)	2519(2)	326(1)	9925(1)	234(6)	185(6)	172(7)	13(5)	39(6)	55(5)
C(11)	311(2)	801(2)	8200(1)	319(8)	320(8)	346(9)	–16(7)	–76(7)	71(6)
C(12)	5896(2)	2958(2)	10716(1)	296(8)	430(9)	360(9)	20(8)	–68(8)	52(7)
C(13)	1109(2)	3440(2)	8979(1)	216(6)	263(7)	242(7)	20(6)	–2(6)	91(5)
C(14)	1910(2)	–986(2)	8506(1)	264(7)	208(6)	212(7)	–9(6)	16(6)	59(5)
C(15)	6305(2)	3159(2)	9030(1)	196(6)	236(7)	344(8)	17(6)	56(6)	67(5)
C(16)	3141(2)	1666(2)	11324(1)	273(7)	239(6)	173(7)	0(6)	2(6)	86(5)
O(1)	11(1)	3365(1)	9329(1)	361(5)	818(7)	674(8)	377(6)	244(6)	396(5)
O(2)	1511(1)	4224(1)	8407(1)	438(5)	449(5)	355(6)	179(5)	87(5)	291(4)
O(3)	2378(2)	–1273(1)	7875(1)	653(8)	258(6)	329(6)	–90(5)	226(6)	34(5)
O(4)	881(2)	–1828(1)	8863(1)	452(7)	239(6)	428(7)	–100(5)	192(5)	–80(5)
O(5)	7100(1)	2359(1)	9077(1)	259(5)	371(6)	1300(10)	225(8)	268(7)	160(4)
O(6)	6792(1)	4280(1)	8858(1)	273(5)	292(5)	636(8)	149(6)	157(6)	44(4)
O(7)	2719(1)	2392(1)	11782(1)	603(6)	413(5)	178(5)	1(5)	78(5)	284(4)
O(8)	3632(2)	734(1)	11572(1)	756(7)	495(6)	197(5)	75(5)	40(5)	421(4)
H(4A)	471(2)	53(2)	894(1)	34(5)					
H(4B)	408(2)	115(2)	818(1)	33(5)					
H(8A)	116(2)	210(2)	1027(1)	25(5)					
H(8B)	252(2)	343(2)	1042(1)	23(4)					
H(9A)	413(2)	422(2)	928(1)	27(5)					
H(9B)	371(2)	339(2)	837(1)	24(4)					
H(10A)	153(2)	–8(2)	1007(1)	27(5)					
H(10B)	314(2)	–20(2)	1008(1)	28(5)					
H(11A)	–29(2)	136(2)	806(1)	43(5)					
H(11B)	2(2)	–5(2)	792(1)	38(5)					
H(12A)	685(2)	336(2)	1055(1)	42(5)					
H(12B)	585(2)	296(2)	1128(1)	49(6)					
HO(2)	89(2)	470(2)	832(1)	62(6)					
HO(4)	52(2)	–260(2)	861(1)	70(8)					
HO(5)	806(3)	283(3)	907(2)	100(10)					
HO(8)	377(2)	76(2)	1211(1)	71(8)					
OW	–446(1)	5600(1)	8187(1)	267(5)	296(5)	241(5)	62(4)	16(4)	83(4)
HW(1)	–68(2)	572(2)	773(1)	61(6)					
HW(2)	–114(3)	528(2)	844(2)	81(9)					

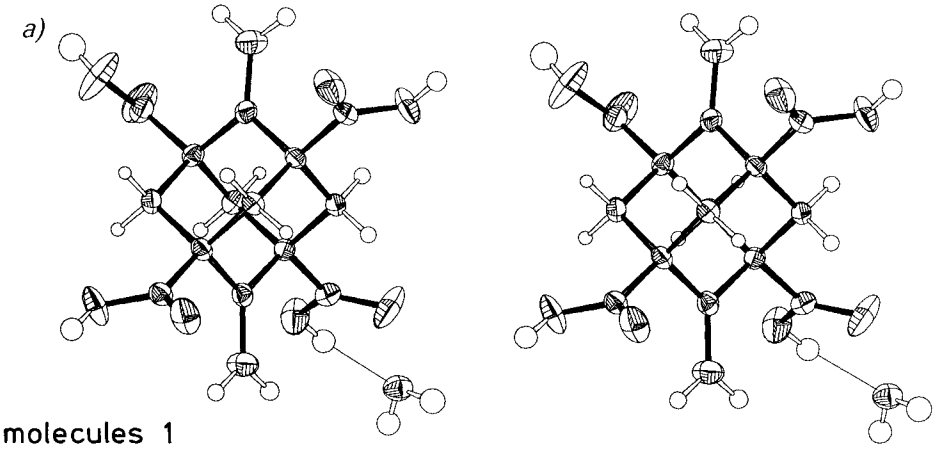

Fig. 14. *Crystal structure of* **4**·H_2O. a) *Stereoviews of both independent tetra-acid molecules* **4** (along C(8)/C(4) axis for right member of stereo pair) *with vibrational ellipsoids* (50% probability, U_{iso} of H-atoms divided by 3). One H_2O molecule H-bonded to a COOH group is also shown; tetra-acid and bonded H_2O are of the same type.

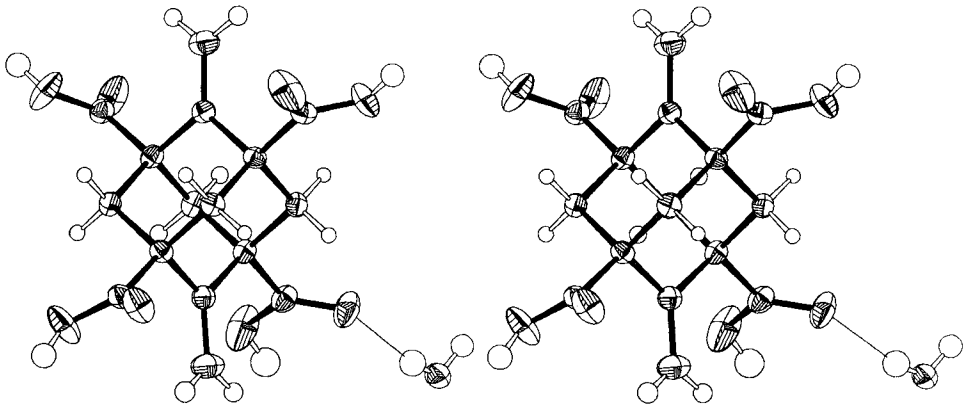

molecules 2

b)

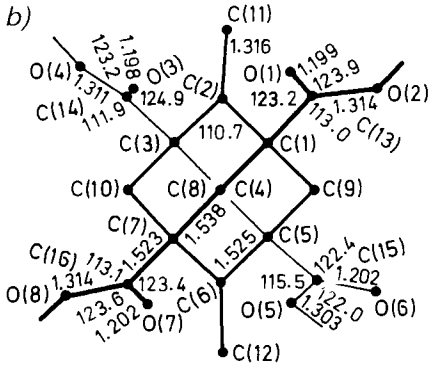

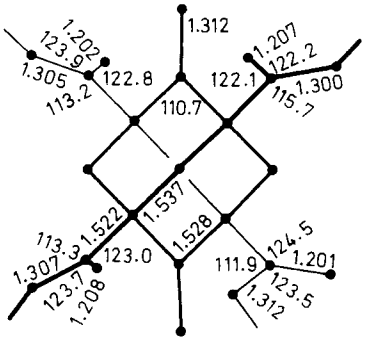

C(2)-C(1)-C(13)-O(2)	-98.3		-97.9
C(2)-C(3)-C(14)-O(4)	-69.8		-86.3
C(6)-C(5)-C(15)-O(5)	85.8		73.7
C(6)-C(7)-C(16)-O(8)	-94.0		-77.0

molecules 1 molecules 2

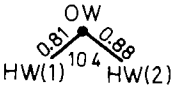

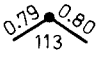

Fig. 14 (*cont.*). b) *Atomic numbering and selected bond lengths* [Å], *bond and torsion angles* [°]. Data of C-skeletons averaged over D_{2d} symmetry; estimated average standard deviations *ca.* 0.002 Å and 0.1°, resp., for tetra-acid, 0.02 Å and 1° for H_2O molecules.

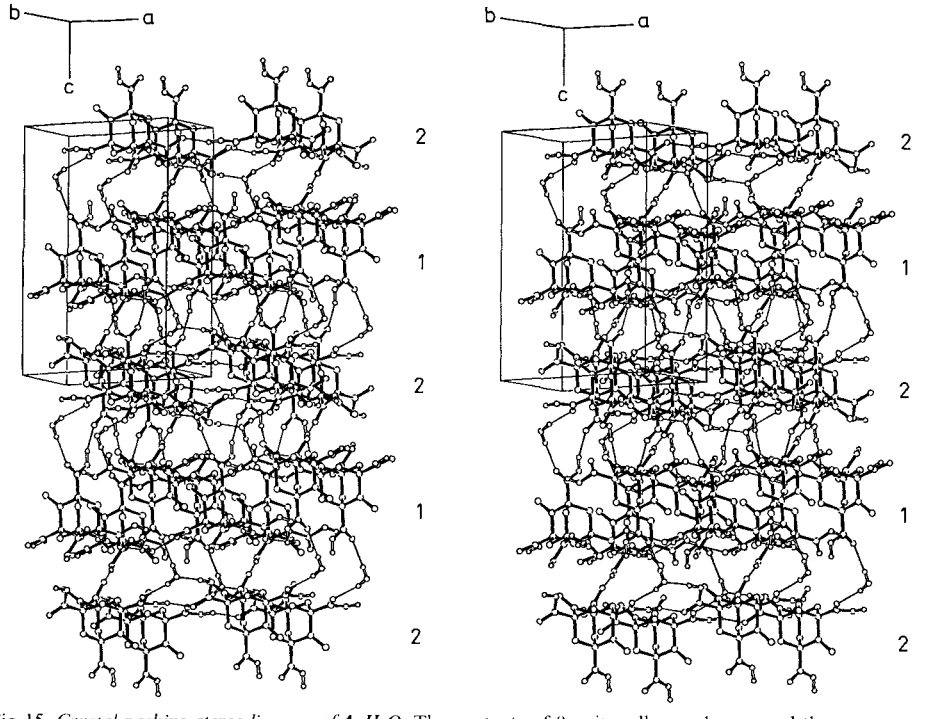

Fig. 15. *Crystal-packing stereodiagram of* **4**·H_2O. The contents of 8 units cells are shown, and the two types of symmetry-independent tetra-acid and H_2O molecules building up the two likewise different kinds of double layers parallel to the *a, b* plane are differentiated by the labels 1 and 2, resp., in the right column.

and *Fig. 14* shows thermal ellipsoids, selected structural data, and atomic numbering. *Fig. 15* shows a space-group symmetry diagram with the contents of 8 unit cells, while the H-bonding environments of **4** and H_2O molecules in **4**·H_2O are depicted in *Fig. 16*. The double-zincblende characteristics of the crystal structure of **4**·H_2O are highlighted in *Fig. 17*, whereas *Fig. 18* illustrates the alternative interpretation in terms of pairwise interpenetrating two-dimensional 4-connected nets. For comparison, *Fig. 19* finally provides stereoviews of three published comparable crystal structures with interpenetrating two-dimensional networks.

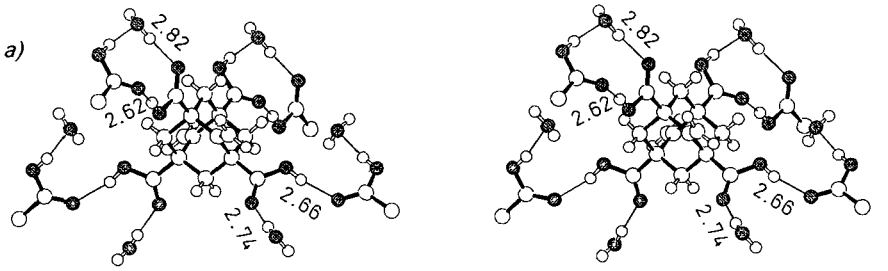

Fig. 16. *H-Bonding environment of the tetra-acid* (a) *and* H_2O (b) *molecules in* **4**·H_2O.

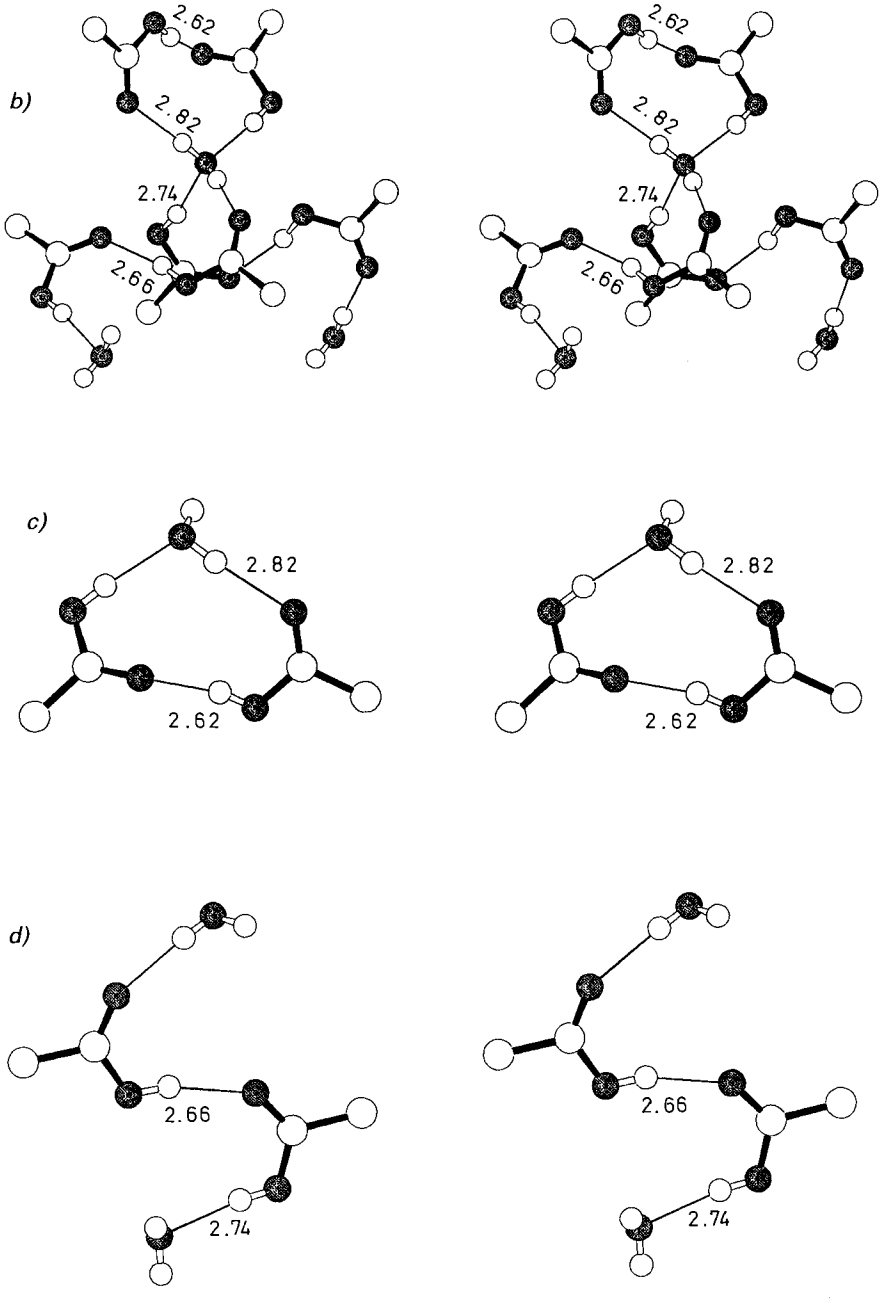

Fig. 16 (*cont.*). The environments of both symmetry-independent types of molecules are very similar, and only those of type 1 tetra-acid and H_2O are shown. This holds similarly for the tilted (*c*) and antiparallel (*d*) variants of the COOH···COOH H-bonds. Average O(H)O distances [Å] of the various kinds of H-bonds are included in the stereodiagrams (O-atoms shaded).

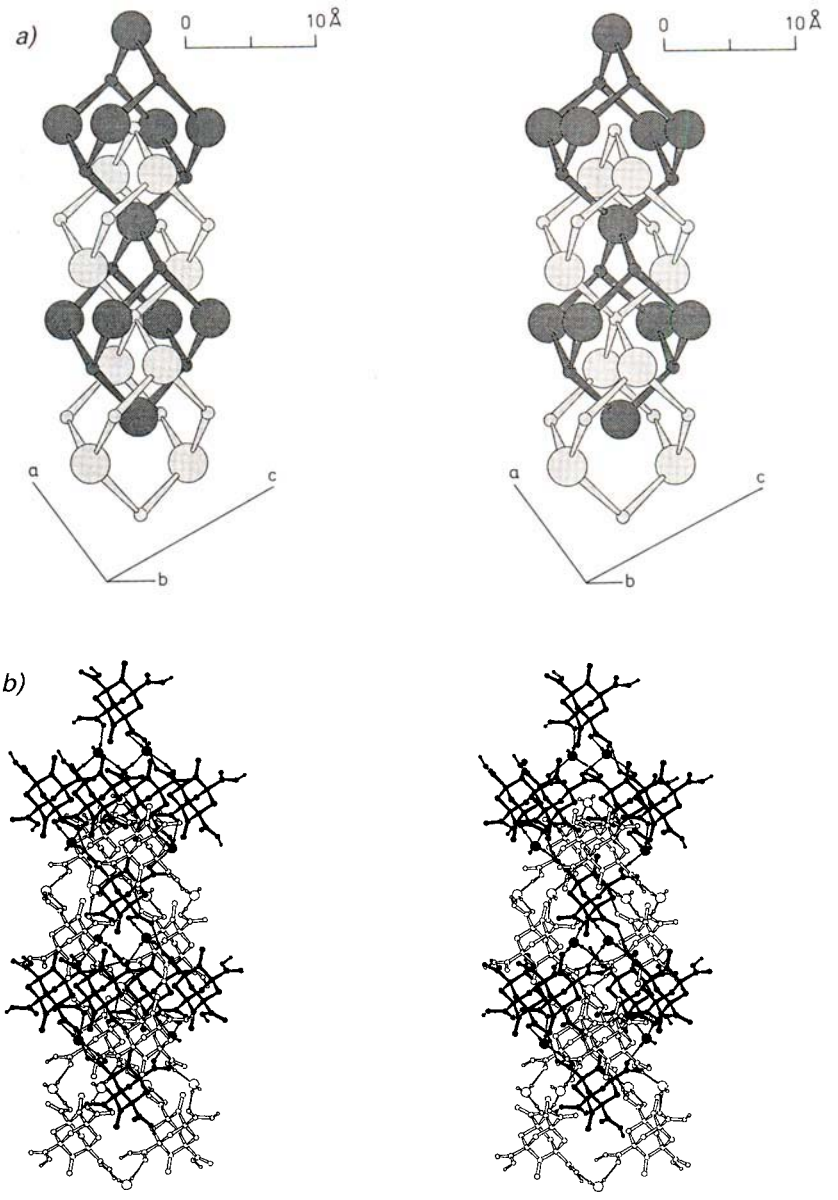

Fig. 17. *Double super-zincblende description of the H-bonded crystal structure of* **4**·H_2O. Scale and orientation of the three stereoviews are the same; the cell axes are indicated. a) *Diagrammatic representation of the double-zincblende architecture defined by the* $H_2O\cdots$COOH H-bonds and represented by two connected super-adamantane units cut out of the two complete, infinite networks (dark and light grey, respectively). The large spheres symbolize the dimethylidenetetetracarboxylic acid molecules at their centers, the small ones stand for the O-atoms of the H_2O molecules. The interconnecting rods represent the $H_2O\cdots$COOH H-bond links. The (antiparallel) COOH$\cdots$COOH H-bonds cross-linking the two interpenetrating networks are not indicated. b) *Ball-and-stick representation.* All H-bonds drawn (thin lines), H_2O O-atoms enlarged for better recognition.

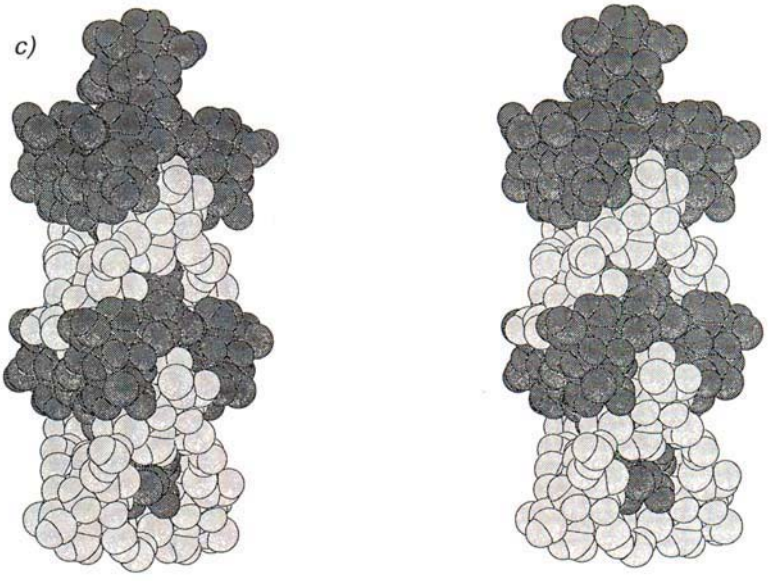

Fig. 17 (*cont.*). c) *Space-filling stereoview.*

Discussion. – 1. *Solid-State Inclusion Compound of Host* **4** *with 4-Methylpent-3-en-2-one (***5***, MP), 2,6-Dimethylhepta-2,5-dien-4-one (***6***, DMH), and Mesitylene (***7***, M) as Molecular Guests* (**4**·(MP-DMH-M). This inclusion compound crystallizes in the tetragonal space group $P4_2/nnm$ (D_{4h}^{12}, No. 134); the unit cell contains 2 molecules of **4**, 1.2 molecules of **5**, 0.2 of **6**, and 2.2 of **7**. Accordingly, the tetra-acid molecules have the rather high (indeed the highest possible) symmetry D_{2d}. Strictly speaking, this represents an average symmetry, since it imposes a twofold orientational disorder on the COOH groups. This may be easily picked up from the space-group symmetry diagram shown in *Fig. 2*; note that the mirror planes cut perpendicularly through the planes of the COOH groups. Intramolecular geometry and temperature motion of **4** are unexceptional in the present complex; *Table 2* and *Fig. 1* provide pertinent information.

A comment is in place regarding the COOH partial conformations of **4**, since we have measured its structure independently altogether six times in the crystalline molecular complexes reported here. The torsional freedom of the COOH groups in **4** is limited due to the methylidene groups, which, for simple sterical reasons, lead to a more or less orthogonal orientation of the COOH planes with respect to the plane of the C=C bonds. Thus, all six observed structures of **4** are conformationally rather similar, and the molecular symmetry is always roughly D_{2d} (see below), irrespective of the fact that this symmetry, which fixes the COOH groups conformationally, is crystallographically imposed on **4** only in **4**·(MP-DMH-M). In all the five other cases reported subsequently, the COOH groups are conformationally restricted only due to physical (sterical) reasons, yet not by crystallographic symmetry requirements. A second comment on the intramolecular structure of **4** in **4**·(MP-DMH-M) concerns the C=C bond length, which appears shortened by a few hundredths of an Å (*Fig. 1b*). This may not be attributed to the limited precision

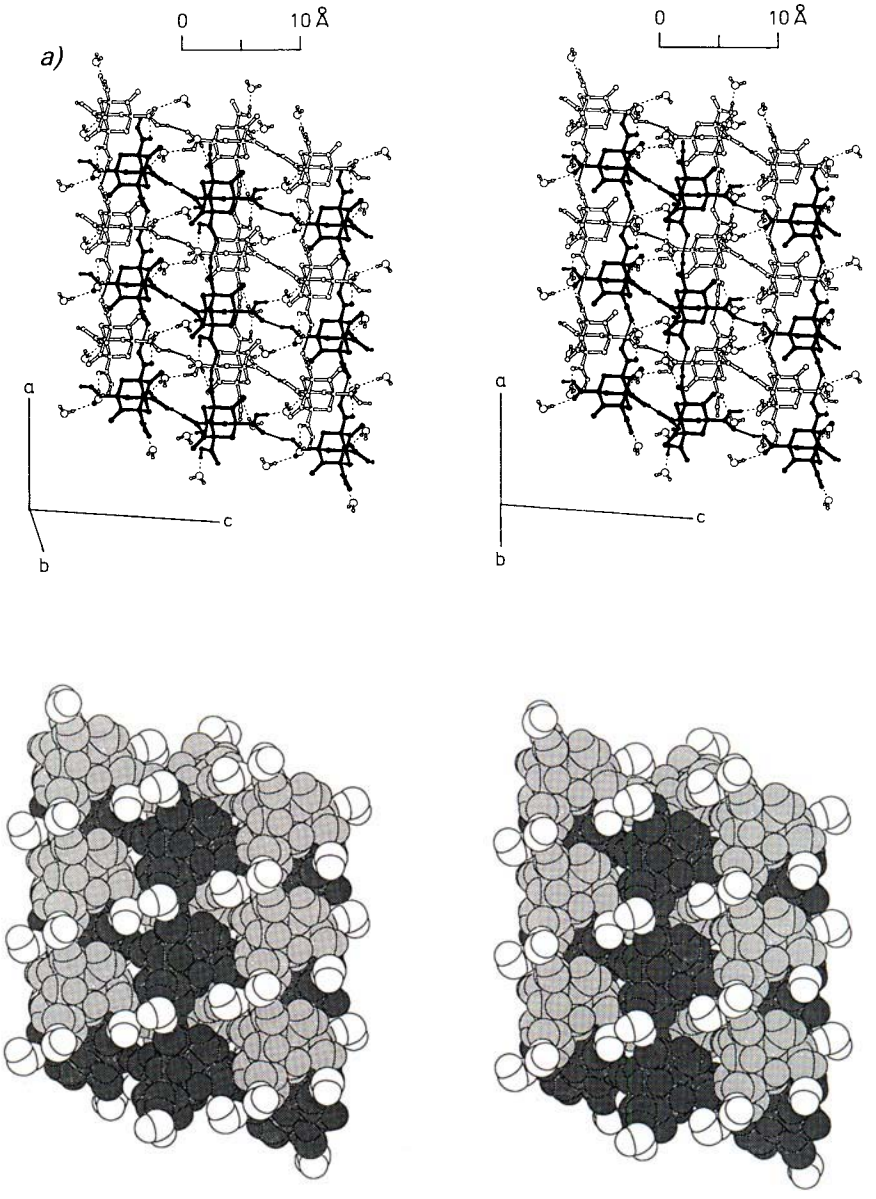

Fig. 18. *Doubly interpenetrating layer description of the H-bonded structure of* **4**·H_2O. a) *Top:* Ball-and-stick stereoview of two interpenetrating, puckered layers (black and white, resp.) represented by four fused 'super-cyclobutane' units cut out of the networks defined by the single COOH···COOH H-bonds (thin lines). Cell axes are indicated. The H_2O molecules and cross-linking H_2O···COOH H-bonds are also shown (thin dashed lines). *Bottom:* same view in space-filling notion; two interpenetrating layers dark and light grey, resp., H_2O molecules white.

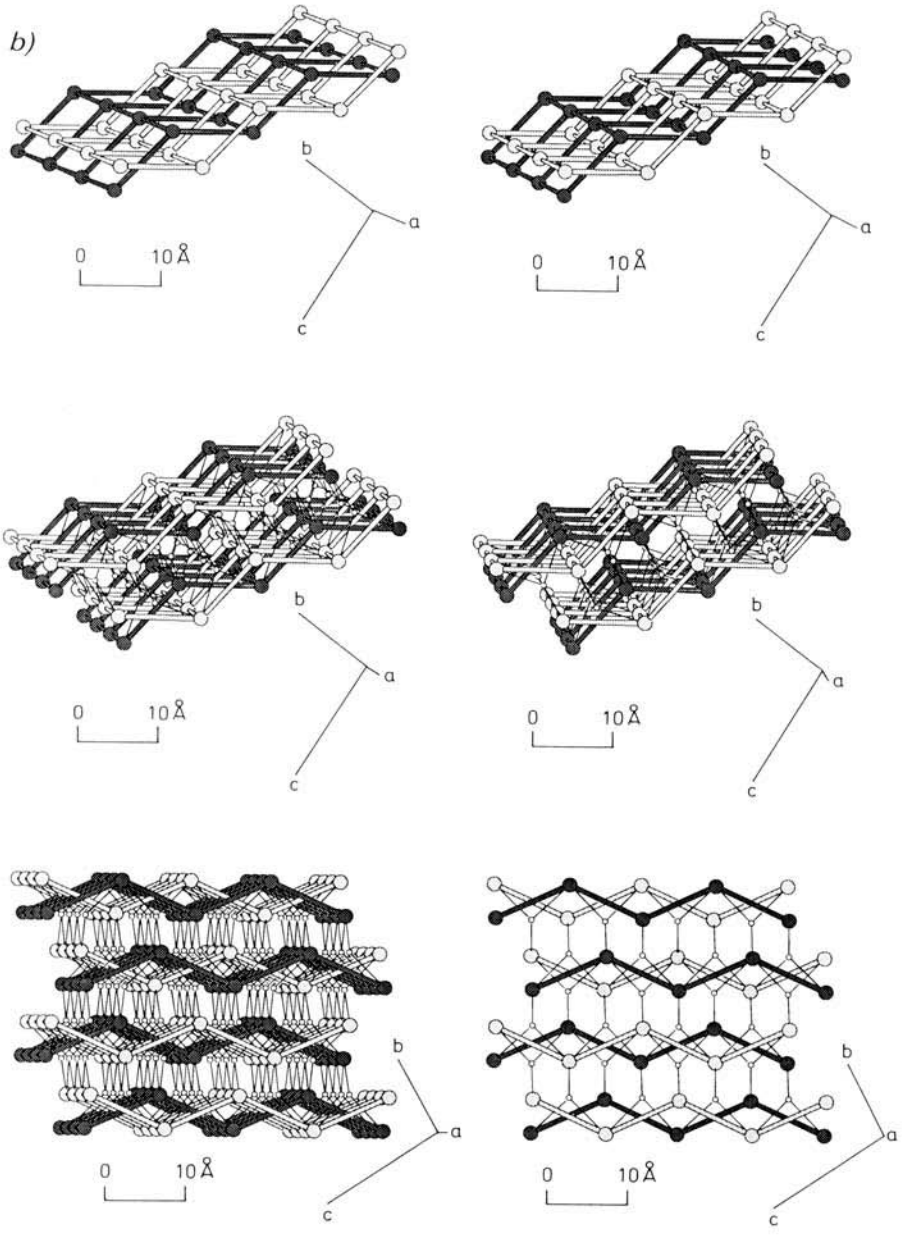

Fig. 18 (*cont.*). b) *Three diagrammatic stereorepresentations of same scale with cell edges outlined.* The large spheres symbolize the dimethylidenetetracarboxylic-acid molecules at their centers, and the interconnecting thick rods stand for the COOH···COOH H-bonds; those along the *a* axis are of the tilted variant, the others of the antiparallel type. *Top:* one double layer consisting of two interpenetrating puckered single layers; H_2O omitted. *Middle:* two adjacent double layers with cross-linking H_2O molecules (small spheres represent H_2O O-atoms) and H_2O···COOH H-bonds (thin lines). *Bottom:* four stacked double layers, side view (right member of stereopair) with cross-linking system of H_2O molecules.

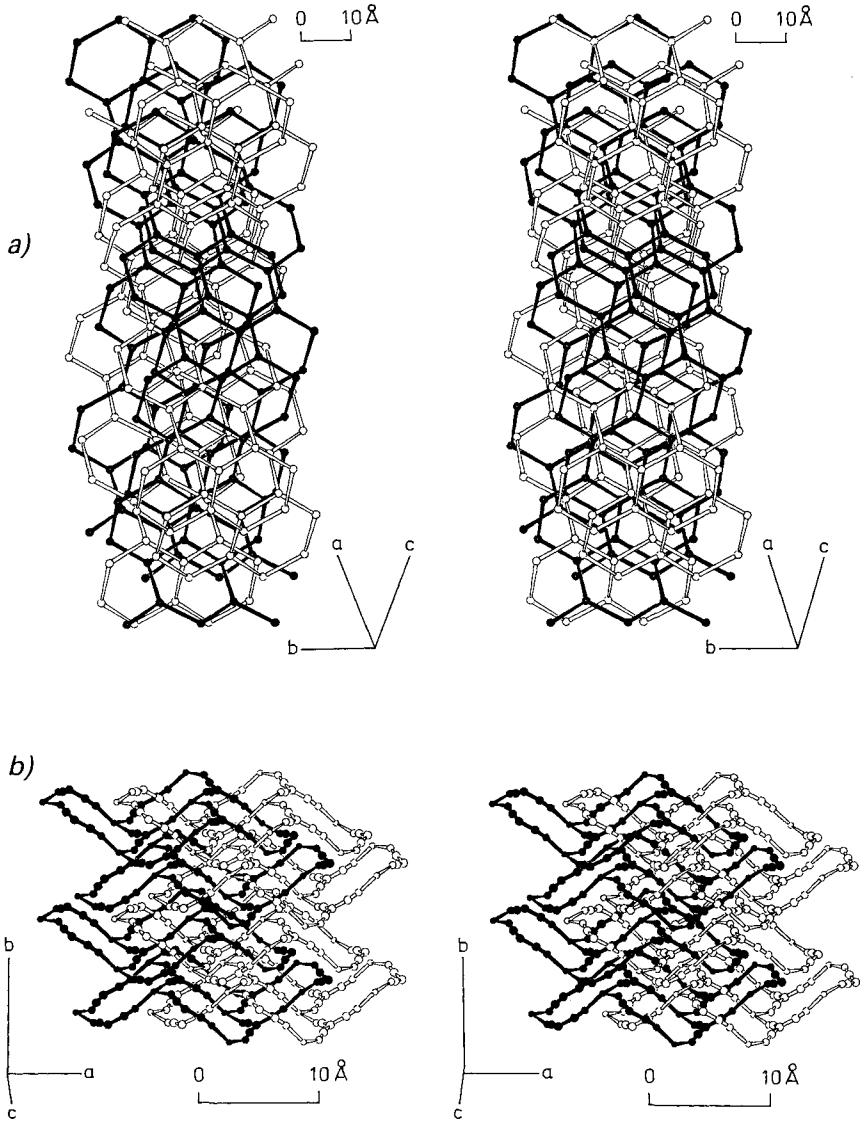

Fig. 19. *Stereoviews of three crystal structures with interpenetrating layer architectures.* Cell edges indicated. a) *Diagrammatic stereoview of the benzene-1,3,5-tricarboxylic-acid* (trimesic acid, TMA) *structure.* Drawing based on the atomic coordinates of [7]. The spheres symbolize the benzene rings at their centers, the interconnecting rods stand for the pairwise H-bonded COOH groups. The TMA structure consists of four sets of puckered, openly stacked 'super-graphite' sheets (wide-meshed hexagonal 'chicken-wire' nets). Sheets of different sets interpenetrate to attain tight packing; altogether the degree of interpenetration is fourfold. In the diagram, two sets of pleated super-graphite sheets are shown comprising three layers each. A complete section of the fourfold interpenetration pattern may be perceived at about the level of the figure label 'a'. b) *Crystal structure of the silver salt of cyanoform, Ag[C(CN)$_3$].* Stereodrawing is based on the atomic coordinates of [8]. The structure is built up of double layers comprising two interpenetrating, puckered 'super-black phosphorus' sheets (dark and white, resp., in the diagram) with alternating trigonal Ag- and C-centers. Four stacked double layers are shown.

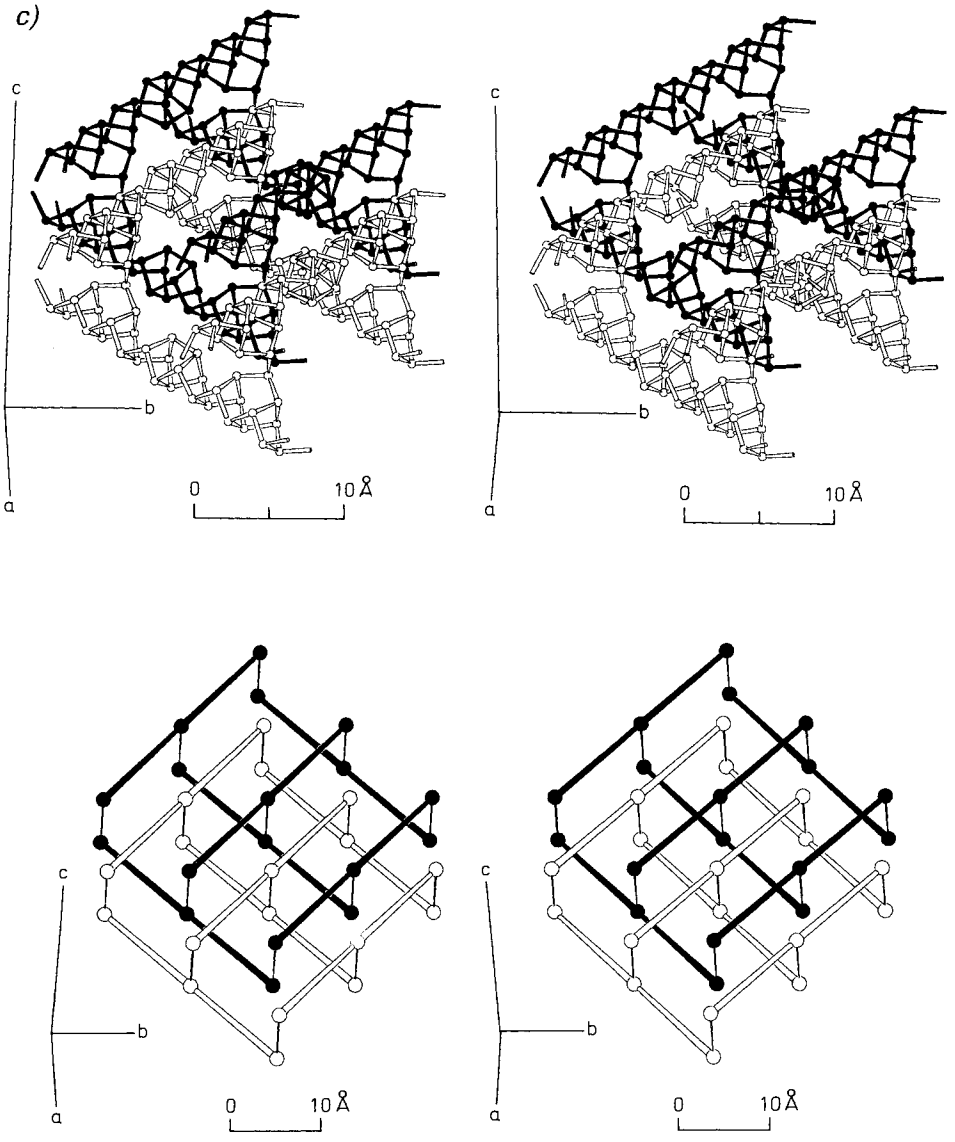

Fig. 19 (*cont.*). c) *Crystal structure of* Hittorf's (monoclinic) *phosphorus*. Stereoviews are based on the atomic coordinates of [9]. The structure is made up of chains with pentagonal cross-section consisting of fused polycyclic P cages. Orthogonal chains are joined by single P–P bonds to form 4-connected sheets consisting of fused 'super-cyclobutane' rings. These sheets interpenetrate pairwise resulting in double layers, which are stacked to build the complete structure. *Top:* ball-and-stick representation of two concatenated super-cyclobutane macrocycles cut out of a double layer. *Bottom:* diagrammatic view of a double-layer portion. The spheres represent the centers of the P_9 cages linked by single P–P bonds (thin lines), and the interconnecting rods symbolize the polycyclic P chains. Both layer sections comprise four fused super-cyclobutane rings.

of the structural data of **4**·(MP-DMH-M), but is observed likewise in the five other cases reported further on (compare in particular the rather precise structures of **4**·M_2 and **4**·H_2O described below). As suggested by shape and size of the vibrational ellipsoids (*Fig. 1a*) and substantiated by more quantitative estimates, the C=C bond shortening in **4** is probably to a significant extent due to thermal motion ('riding' motion of the *exo*-methylidene groups).

The guest molecules **5**–**7** present in **4**·(MP-DMH-M) are disordered to the extent that no refinable structural model could be delineated for them by difference *Fourier* methods (see *Experimental*). Consequently, the following discussion of **4**·(MP-DMH-M) is entirely focussed on the novel and intriguing double-diamond-like architecture of the tetra-acid host.

The molecules of the tetrahedral tetra-acid **4** join to form two symmetrically interpenetrating super-diamond networks in the present inclusion compound **4**·(MP-DMH-M), *via* the usual pairwise H-bonds between the COOH groups. The carboxylic linkages are located on crystallographic sites of symmetry C_{2h}. Their O(H)O distance is 2.659(14) Å, and the separation between two H-bonded molecular centers amounts to $\frac{1}{2}(2a^2 + c^2)^{\frac{1}{2}} = 9.983$ Å (*Fig. 2*). The diamond-like networks are somewhat compressed tetragonally by a factor of c/a = 0.9256. Both interpenetrating, yet otherwise unconnected networks are translationally equivalent and may be merged into one another by executing the elementary translations a, b, or c. Note that the tetra-acid molecules have the exocyclic C=C bonds oriented along the tetragonal *c* axis, as exacted by their crystallographic D_{2d} symmetry. Ball-and-stick and space-filling stereorepresentations of the beautiful double-diamond host architecture of **4**·(MP-DMH-M) are shown in *Fig. 3*. It may be seen that both diamond-like host networks have no close *van-der-Waals* contacts and are evidently almost totally embedded in the disordered guest molecules, functioning much like a glassy matrix. This is in contrast to the inclusion compound **3**·AcOH mentioned in the introduction, which is characterized by triply helical host channels accommodating chains of AcOH guest species [2].

The space group $P4_2/nnm$ taken up by the inclusion compound **4**·(MP-DMH-M) is rather rare, and the only other prominent example is provided by the tetragonal boron allotrope T-50 (α-tetragonal B with cell constants $a = 8.756$, $c = 5.078$ Å, and 50 B-atoms per unit cell) and a number of closely related derivatives [3] [10] [11]. Thorough inspection of the crystal structure of this tetragonal form of B-atom leads to the remarkable (and hitherto apparently unnoticed) perception that it may very convincingly be described in terms of a double-diamond architecture, which turns out to be completely analogous to that of the host structure of the present inclusion compound **4**·(MP-DMH-M). The double-diamond structure of T-50 B may readily be developed from that of **4**·(MP-DMH-M) through replacing the tetrahedral tetra-acid molecules by (tetragonally compressed) tetrahedral tetravalent B-atoms with D_{2d} site symmetry, and the carboxylic linkages by icosahedral B_{12} bridging units with site symmetry C_{2h}. Whereas in **4**·(MP-DMH-M) the tetrahedral units are bulkier than the bridges, this is reversed in T-50 B. However, it should be noted that in T-50 B additional B–B bonds occur both within each of the two diamond-like frameworks and between them (cross-linked double-diamond structure; the B-atoms forming the icosahedra are hexavalent). Thus, in T-50 B altogether the following differentiations may be made with respect to various types of B-atoms and B–B bonds: icosahedral, hexavalent *vs.* tetrahedral, tetravalent B-atoms;

intraicosahedral *vs.* extraicosahedral B–B bonds, intradiamond-like *vs.* interdiamond-like (cross-linking) B–B bonds.

Illustrations are provided in *Fig. 4* showing a space-group symmetry diagram (to be compared with *Fig. 2*) of T-50 B and a pictorial stereorepresentation of its fascinating double-diamond architecture. It is seen to be compressed tetragonally (by a factor of 0.5799), more so than the analogous structure of **4**·(MP-DMH-M). Considering the enormous hardness of boron, which is second only to diamond, it is thus reassuring to note that its crystallography includes diamond-like aspects. The analogy between the present inclusion compound **4**·(MP-DMH-M) and T-50 B may even be carried one step further: the double-diamond structure of this B allotrope as sketched above has small tetrahedral holes of site symmetry D_{2d} in between the B_{12} icosahedra, which may accommodate (tightly bound) 'guest' atoms like C, N, Ti, and V. In fact, it has repeatedly been claimed that the structure of T-50 B is only stable if supported by these atomic guests (see [11] and lit. cit. therein). Accordingly, there is good reason to view T-50 B as an inorganic inclusion compound, much like **4**·(MP-DMH-M), whose organic H-bonded double-diamond host architecture clearly cannot possibly exist without the stabilizing matrix of the guest molecules **5**–**7**.

The unit cell of **4**·(MP-DMH-M) is approximately cube-shaped, since $a \approx c$. Exact cubic symmetry is of course not possible, because **4** lacks threefold axes. If these were present, then the highest symmetry possible for a double-diamond structure could be adopted, which corresponds to the cubic space group $Pn\bar{3}m$ (O_h^4, No. 224). The prototypal double-diamond structure of this cubic symmetry is that of cuprite Cu_2O. The two undistorted, translationally equivalent super-diamond networks of cuprite are built up by tetrahedral oxygen ions (site symmetry T_d) linked across linear Cu bridges (site symmetry D_{3d}); *Fig. 5* provides illustrations with more details. Formally, it may be stated that $P4_2/nnm$, the tetragonal space group of our present inclusion compound **4**·(MP-DMH-M), represents a maximal non-isomorphic subgroup (index 3, 'translationengleich') of the cubic cuprite space group $Pn\bar{3}m$; this becomes particularly clear, if one compares the corresponding full space group symbols $P4_2/n2/n2/m$ and $P4_2/n\bar{3}2/m$ (*Figs. 2* and *5a*; see [12] [13] for more general and rigorous treatments of group-subgroup relations among crystallographic space groups). Therefore, it appears that the tetragonal space group $P4_2/nnm$ adopted by **4**·(MP-DMH-M) represents the highest possible crystallographic symmetry attainable by a double-diamond structure of a tetrahedral tetracarboxylic acid in general. It is finally noted that generally inorganic double-diamond structures are not particularly rare, and quite a few further examples could be cited (see [1] and [14], in particular footnotes 6 and 8, resp.).

2. *Solid-State Inclusion Compound of* **4** *with Mesitylene as Molecular Guest* (**4**·M_2). This second inclusion compound of **4** has exclusively mesitylene guest molecules with a host-guest ratio 1:2. Like **4**·(MP-DMH-M), the present complex **4**·M_2 also crystallizes tetragonally, yet in the different space group $I4_1/acd$ (D_{4h}^{20}, No. 142). The unit cell contains 8 molecules of **4** and 16 molecules of **7**. The tetra-acid host molecules have crystallographic D_2 symmetry, and the mesitylene guest species are residing on C_2 axes of symmetry (*Fig. 7*). Except for the usual twofold torsional disorder of the COOH groups and the orientational disorder of the mesitylene Me group on the C_2 axis, the structure of **4**·M_2 is essentially ordered. Intramolecular geometry and temperature motion of host and guest of **4**·M_2 (*Table 3*, *Fig. 6*) do not require much detailed discussion *per se*, yet are of interest

in comparison with the partially disordered structure of the third inclusion compound **4**·(MP-M) described later.

As already discussed in the context of the previous inclusion compound **4**·(MP-DMH-M), the COOH partial conformations of **4** are similar in the present complex **4**·M_2. In fact, the molecular D_{2d} symmetry of **4** imposed crystallographically in **4**·(MP-DMH-M) (see above), is very closely approximated in **4**·M_2 as testified by the torsion angles given in *Fig. 6c*. As indicated earlier, too, the C=C bonds of **4** in **4**·M_2 are again shortened (to 1.303(5) Å), presumably in substantial measure due to thermal motion. Similar apparent C=C bond contractions are met in the other complexes of **4** discussed subsequently.

Like in **4**·(MP-DMH-M), the tetra-acid molecules of the present complex **4**·M_2 build up two equivalent, symmetrically interpenetrating super-diamond networks *via* pairwise H-bonds between the COOH groups. The diamond-like host networks in **4**·(MP-DMH-M) and **4**·M_2 are closely symmetry-related, since the space group of the latter, $I4_1/acd$, is a subgroup of $P4_2/nnm$ (index 2, 'klassengleich') [12] [13]. Accordingly, the symmetry of the host lattice in **4**·(MP-DMH-M) is higher than in **4**·M_2 (*Figs. 2* and *7*). Thus, the (average) site symmetry of the COOH linkages is C_{2h} in the former case but only C_i in the latter; similarly, the crystallographic symmetries of the tetra-acid molecules (D_{2d} and D_2, respectively) comply with a group-subgroup relationship. However, the overall dimensions of the super-diamond lattices are very similar in both cases. The O(H)O distance in **4**·M_2 is 2.667(5) Å and two H-bonded tetra-acid molecules are $\frac{1}{4}(4a^2 + c^2)^{1/2} = 10.005$ Å apart; the super-diamond networks are tetragonally very slightly elongated by a factor of $c/(\sqrt{2}\,a) = 1.0264$. The ordered uptake of the mesitylene guest molecules in **4**·M_2 is thus seen to occur within an almost undistorted double-diamond-like host structure.

Although, as we have seen, the diamond-like host lattices of **4**·M_2 and **4**·(MP-DMH-M) are largely similar, two main differences should be noted (*Figs. 2*, *3*, *7*, and *8*). Whereas the two interpenetrating diamond-like networks of **4**·(MP-DMH-M) are translationally equivalent, those of **4**·M_2 are not, and whereas the exocyclic C=C bonds of **4** are oriented along the tetragonal *c* axis in the former complex, they are perpendicular to the *c* axis in the latter. The two symmetry-equivalent super-diamond lattices of **4**·M_2 are related *e.g.* by 4_1 screw axes, or by C_2 axes directed along *a* or *b*; this means that within one super-diamond lattice the C=C bonds are oriented parallel to one diagonal in the *a*, *b* plane and within the second diamond lattice parallel to the other, perpendicular diagonal in the *a*, *b* plane (*Figs. 7* and *8c*, *d*).

The discussion of the arrangement of the mesitylene guest molecules in **4**·M_2 is facilitated by inspection of *Fig. 7* and, in particular, *Fig. 8* providing various stereoviews of the intriguing architecture of this double-diamond-like solid-state inclusion compound. The disposition of the mesitylene guests may be characterized in two ways: *a*) the mesitylene molecules may be grouped into helices of alternating chirality winding about the 4_1 screw axes. Necessarily, there are 4 mesitylene molecules per turn, and the rise of the helix per turn (pitch) is equal to the cell edge *c*, and thus also equal to the distance between two opposite centers of a super-adamantane unit of the host. One Me group of each mesitylene molecule, *i.e.* that on a twofold axis, is 'anchored' approximately on the 4_1 screw axis (*Fig. 7*). *b*) The mesitylene molecules may alternatively be grouped into orthogonal chains running along the C_2 axes (parallel to the cell edges *a* and *b*) on which the guest species are located. Along these chains, the mesitylene molecules are lined up in

a head-to-tail fashion controlled by the glide planes *a* and *b* perpendicular to the cell edge *c*. These glide planes produce an alternating tilt of the molecular planes of the guest molecules, which follows that of the COOH linkages of the host. It may be seen from *Figs. 8b–d* that in this way the mesitylene guests snugly fit in between the two super-diamond networks of the tetra-acid host. The individual mesitylene chains are obviously polar, but the polarity of neighboring parallel chains is opposite as required by the centrosymmetric space group. As a whole, the host-guest complex **4**·M_2 displays a rather intricate pattern of multiple interpenetration consisting of the two interlaced super-diamond host networks, which are themselves interpenetrated by two sets of non-intersecting mesitylene chains crossing each other at right angles (*Fig. 8*). As in **4**·(MP-DMH-M), the two host networks of **4**·M_2 have no *van-der-Waals* contacts and are totally bathed in the matrix of aromatic guest molecules sandwiched in between. However, contrary to **4**·(MP-DMH-M), the intercalating three-dimensional array of guest molecules is ordered in the crystals of **4**·M_2.

The space group $I4_1/acd$ is not particularly rare, and quite a few other cases with this crystal symmetry may be uncovered to incorporate double-diamond-like features. In the following, we briefly discuss three pertinent examples of this space group (*Fig. 9*), which are closely related to the structure of the present inclusion compound **4**·M_2. It is noted that these structures were retrieved from the *Cambridge Structural Database* [15] by simply using the space group number as search criterion; the *Inorganic Crystal Structure Database* [16] offers similarly useful search possibilities. It is also noted that the super-tetrahedral characteristics of the following crystal architectures went unnoticed by their original authors. Uncovering them is not trivial and, therefore, represents a true piece of comparative crystal-structural research important for classification of structural chemistry in general. What follows is thus more than simple structural reviewing.

An inclusion compound of a dimethylhomoadamantanediol with benzene as guest molecules has been reported (host-guest ratio 4:1), which crystallizes in space group $I4_1/acd$ with 32 diol molecules in the unit cell [4a]. Closer inspection of this structure reveals the diol host to be of a double-diamond-like nature in a tetragonally compressed fashion (*Fig. 9a*, compression factor 0.5802). The tetrahedral building blocks are made up of O(H)O H-bonded macrocyclic diol tetramers of S_4 symmetry bridged by pairwise H-bonds (across C_2 sites) to form two symmetrically interpenetrating super-diamond networks, much as in **4**·M_2 with the corresponding site symmetries D_2 and C_i, respectively (see above; in terms of super-diamond architectures, the spacial disposition of both sets of symmetry sites is analogous). The partially disordered benzene guests reside on D_2 sites in between the tetrameric host macrocycles stacked along the tetragonal *c* axis such that altogether a channel-inclusion structure results. The channels, however, have bottle-necks at the S_4 sites, which cannot be passed by the benzene molecules.

It is interesting to note that the same above-mentioned dimethylhomoadamantanediol, when crystallized from AcOEt, forms a channel inclusion compound of a different kind in the trigonal space group $P3_121$, which was also observed for other related diol hosts [4a, b]. Analysis of these trigonal diol host architectures with double-helical channels shows that they are intimately related to the structure of the low-temperature (α) form of quartz, which also takes up space group $P3_121$. We may, therefore, very convincingly refer to these H-bonded diol networks as 'super-quartz' lattices. Their tetrahedral

building blocks (replacing the Si-atoms of quartz) consist of the hydrocarbon cores of the diol molecules plus the two O-atoms from which four H-bridges radiate with distorted tetrahedral directionality (replacing the covalent O-bridges in quartz). Finally, it is worth mentioning in the present context that still another related diol (a diethylbicyclo-[3.3.1]nonanediol) was found to build up a three-dimensional network (without guest molecules) different from the two mentioned above, the space group being *Fdd*2 this time [4c]. This network may be recognized as a single super-diamond structure with H-bonded $(OH)_4$ rings as tetrahedral building blocks, which are bridged by the divalent hydrocarbon cores in diamond-like fashion. The architecture is symmetry related to the super-diamond structure of KH_2PO_4, the low-temperature form of which also crystallizes in the polar space group *Fdd2* [4d]. Still closer is the relationship with the structure of one crystal form of all-*trans*-cyclobutane-1,2,3,4-tetracarboxylic acid, which we have analyzed recently by X-ray methods [4e]. Of this tetra-acid, we characterized two different orthorhombic forms of space group *Pbca* and *Fddd*, respectively, both with eight molecules in the unit cell. The *Pbca* polymorph may be viewed as a cross-linked, distorted double-diamond structure with a rather unusual pattern of H-bonding. The *Fddd* polymorph has a clear-cut triple-diamond structure (threefold interpenetration without cross-linking) brought about by the usual pairwise intercarboxylic H-bonds. The super-diamond networks of this *Fddd* form of the all-*trans*-cyclobutane-1,2,3,4-tetracarboxylic acid now resemble very much the respective architecture of the above-mentioned single super-diamond diol structure in the sense of an inverse covalent/non-covalent relationship: the tetrahedral building blocks of the tetra-acid consist of the covalently bonded, all-*trans*-configurated cyclobutane rings as compared to the H-bonded $(OH)_4$ rings of the bicyclononanediol, from which the alcoholic C–O bonds also emanate in all-*trans*-disposition. Conversely, the H-bonded intercarboxylic bridging elements of the tetra-acid have the covalent hydrocarbon links as their counterpart in the diol.

An ethylenediamine (en) cyano complex of cadmium, $[Cd(en)Cd(CN)_4]$, which crystallizes in space group $I4_1/acd$ with 16 formula units per unit cell [5], may also be shown to take up a double-diamond-like structure. Tetrahedral building blocks consisting of two formula units may be identified, which form 12-membered rings composed of four alternating Cd ions and CN groups. These 12-rings reside on sites of symmetry D_2 and are linked by pairwise CN bridges (across centers of symmetry) to build up two separate, symmetrically interpenetrating superdiamond networks, which are tetragonally somewhat elongated by a factor of 1.1700 (*Fig. 9b*). Half of the Cd ions are additionally coordinated by chelating en ligands. Disregarding the bridging (CN) and chelating (en) ligands, the super-diamond networks may schematically be viewed as three-dimensional arrays of large, fused four-membered Cd_4 rings of which one third function as tetrahedral centers and two thirds as interconnecting bridges. The super-diamond networks of this Cd complex are thus recognized to have exactly the same symmetry properties as those formed by the host **4** in our present inclusion compound $\mathbf{4}\cdot M_2$.

The third example related to $\mathbf{4}\cdot M_2$ concerns dimethylmalonic acid $C(CH_3)_2(COOH)_2$, which also crystallizes in space group $I4_1/acd$ and has 16 molecules in the unit cell [6]. The crystal structure of this diacid is very neatly comparable to the arrangement of the mesitylene guest molecules in $\mathbf{4}\cdot M_2$ and may be developed out of the latter simply through replacing the 16 C_2-symmetric mesitylene molecules in the unit cell by 16 likewise C_2-symmetric dimethylmalonic acid molecules and removing the tetra-acid host

molecules. It was noted above that the mesitylene guests of **4**·M_2 may be grouped into helices winding about the 4_1 screw axes. Of course, the same is true for the dimethylmalonic-acid molecules, and here this structural characterization is physically particularly meaningful, since the diacid species are linked by pairwise H-bonds between the COOH groups in precisely that helical fashion (*Fig. 9c*).

3. *Solid-State Inclusion Compound of* **4** *with 4-Methylpent-3-en-2-one* (**5**, MP) *and Mesitylene* (**7**, M) *as Molecular Guests* (**4**·(MP-M)). This third inclusion compound of **4** is structurally very similar to **4**·M_2 described in the previous section. In addition to mesitylene **7**, **4**·(MP-M) contains a minor amount of **5** as guest molecules; the ratio **4**/**5**/**7** is *ca.* 1:0.4:1.6. The inclusion compounds **4**·(MP-M) and **4**·M_2 crystallize in the same space group ($I4_1/acd$), and their cell dimensions are practically the same (see *Experimental*). Accordingly, the double-diamond-like host structures of both complexes agree within experimental error (*Tables 3* and *4*), and no further discussion is required.

The non-stoichiometric amount of **5** present in **4**·(MP-M) leads to partial disorder, which expresses itself in structural distortions and excessive thermal parameters of the refined mesitylene model assumed to account for the average electron density of both different guest molecules (see *Experimental*). *Fig. 10d* shows that the C–C bond lengths of the disordered mesitylene model of **4**·(MP-M) are *longer* (despite the large thermal parameters!) than those of the essentially ordered mesitylene structure of **4**·M_2 (*Fig. 6d*) by *ca.* 0.03 Å. Furthermore, the CCC angles in the (planar) six-membered ring of the disordered guest model are appreciably widened at the Me positions leading to a more trigonal benzene ring; the other six-ring angles are compressed accordingly. The thermal parameters of the disordered guest model of **4**·(MP-M) are very substantially larger than those in **4**·M_2 (by an average factor of 2.7 for the diagonal elements U_{ii}, *Tables 3* and *4*) and indicate pronounced radial displacements at the unsubstituted C-atoms of the six-membered ring of the mesitylene model (*Fig. 10b*). All these anomalies may be qualitatively accounted for by invoking a sixfold orientational disorder of the MP species as illustrated in *Fig. 10e*. Symmetric, trigonal superposition of the six preferred MP orientations (plus mesitylene itself) leads to a disorder model of average D_{3h} symmetry with structural distortions and atomic displacements similar to those suggested by experiment. It should be noted, however, that this symmetric disorder model is as simple as possible and more pictorial then quantitative. For example, a planar heavy-atom skeleton is assumed for MP with a C=C–C=O torsion angle of 0°, while a moderately non-planar structure might be more appropriate. Furthermore, the averaged bond lengths of the MP model have been chosen equal.

4. *Solid-State Inclusion Compound of* **4** *with (*tert*-Butyl)benzene as Molecular Guest* (**4**·TBB). This fourth inclusion compound of **4** structurally characterized by us has (*tert*-butyl)benzene (**8**) as molecular guest with a non-stoichiometric host-guest ratio of *ca.* 1:1.7. The conventional space group of **4**·TBB is $C2/c$. Instead, we made the unconventional choice $F2/d$, since the associated doubled unit cell is approximately cube-shaped (see *Experimental*) bringing about the relationship with the structure of diamond itself; a space-group symmetry diagram in $F2/d$ is shown in *Fig. 12*. The space group $F2/d$ is readily seen to be a subgroup of the cubic diamond space group $Fd\bar{3}m$ by considering the following desymmetrization sequence (conventional space groups in parentheses): $Fd\bar{3}m \rightarrow F4_1/ddm(I4_1/amd) \rightarrow Fddd \rightarrow F2/d(C2/c)$ (*cf.* [12] and note that space group *Fddd* is taken up by the diamond-like inclusion compound **3**·AcOH [2] mentioned in the

Introduction, and by one polymorph of all-*trans*-cyclobutane-1,2,3,4-tetracarboxylic acid [4e], which forms a triple-diamond structure and was reported in the previous section on **4**·M_2). The all-face centered unit cell of **4**·TBB contains 16 molecules of the host **4** and 27.2 guest molecules of **8**. The host molecules **4** occupy general positions and, therefore, have no crystallographic symmetry. As described in the *Experimental,* the guest molecules **8** are highly disordered, and no sensible structural model could be refined. A discussion of temperature motion and intramolecular geometry of the host **4** in the present complex **4**·TBB would not furnish any new aspects and may be dispensed with; basic refinement results are collected in *Table 5* and *Fig. 11*.

As pointed out in the *Introduction*, we had originally hoped that the replacement of mesitylene by the bulkier (*tert*-butyl)benzene as molecular guest might open a possibility to enforce a single super-diamond network of the host **4**. Such an architecture would be extremely hollow and would, therefore, have led to an inclusion compound with a very large proportion of guest material. However, the actual crystal-structure analysis of **4**·TBB taught us that apparently a better alternative for accommodation of the (*tert*-butyl)benzene guest still exists within a less hollow double-diamond-like host architecture. Both super-diamond lattices are equivalent and may be transformed into each other by twofold axes or symmetry centers. The doubly H-bonded COOH linkages do not possess crystallographic symmetry; within one and the same super-diamond lattice the COOH groups are related by the 'diamond' glide planes *d* (*Fig. 12*). All C=C bonds of the host molecules **4** are essentially parallel and oriented along the crystallographic axis *a*.

Whereas replacement of the mesitylene guest molecules in **4**·M_2 by (*tert*-butyl)benzene (leading to **4**·TBB) does not change the double-diamond-like nature of the tetra-acid host architecture, *i.e.* its *degree* of interpenetration, this does not hold for the *mode* of interpenetration. In **4**·M_2 (as well as in **4**·(MP-DMH-M) and **4**·(MP-M)), the two super-diamond networks of the host interpenetrate symmetrically, *i.e.* they are shifted with respect to one another by half the distance between two opposite tetra-acid molecules of a super-adamantane unit, and they do not experience *van-der-Waals* contacts. However, in **4**·TBB the increased steric bulk by the *t*-Bu group effects an asymmetric interpenetration of the host such that the two super-diamond networks ar moved towards each other to within *van-der-Waals* contact. The shift vector relative to the symmetric interpenetration is 0.136**a** + 0.124**c** and has a length of 4.21 Å (*Figs. 12* and *13*; note that this vector is perpendicular to the *b* axis and has thus no component in **b**, since the two interpenetrating super-diamond lattices are transformed into one another by crystallographic twofold axes along *b*). In this way, the previously even (symmetric) distribution of hollow host spaces between the two diamond lattices is broken such that one half of the cavities grows at the expense of the other half. In fact, one half of the cavities vanishes altogether, *i.e.* the two super-diamond networks attain *van-der-Waals* contact. An intermediate situation would be unfavorable, since the smaller cavities could not accomodate guest material any more and would have to remain empty. The asymmetry shift of the two diamond-like lattices in **4**·TBB is, therefore, maximal and follows an all-or-nothing principle: the interstices are either large enough to house molecular guests or they vanish completely! The expanded cavities in **4**·TBB are thus seen to provide sufficient room for accommodation of the bulky TBB guest molecules without disrupting the double-diamond-like host architecture. As evidenced by the cell dimensions of **4**·TBB (see *Experimental*) and *Figs. 12* and *13*, the asymmetry of interpenetration enforced by the

TBB guest molecules does not lead to any pronounced distortion of the two individual super-diamond host lattices. We abstain from discussing further related, but not really necessary details and refer the reader to *Figs. 12* and *13*, which provide a sufficiently quantitative impression of the asymmetric double-diamond-like host structure of **4**·TBB by means of a unit-cell projection and a number of stereoviews. The actual shape of the host cavities in **4**·TBB is discussed after the following paragraph.

Within a few tenths of an Å, the asymmetry shift of 4.21 Å between the two super-diamond networks of **4**·TBB amounts to half the diameter of the adamantane core of our present tetrahedral host **4**. This observation leads to the rough estimate that in order to break the double-diamond structure of **4** and, thus, in order to favor a single-diamond host architecture, the guest molecules should at least be more voluminous (bulky) than the adamantane molecule. More precisely, their smallest diameter should be larger than the diameter of adamantane. If a single-diamond-like inclusion compound of host **4** could be realized with smaller guest species, this would have to be considered as a sheer matter of luck rather than systematic supramolecular design, made possible *e.g. via* a particularly favorable yet hardly predictable fit of host and guest molecular shapes. The adamantane bulk estimate as a lower guest volume limit for a designed breaking of the double-diamond structure of **4** may also qualitatively be arrived at by considering the fact that the asymmetric twofold diamond-like interpenetration of **4**·TBB is to a certain extent similar to that generated out of the symmetric triple-diamond interpenetration of **3**·AcOH [2] (see *Introduction*) by removing one diamond-like host lattice. This topological correspondence is brought about particularly clearly by the diagrammatic and space-filling stereoviews shown in *Figs. 13a* and *b*, which should be compared with Fig. 3 of [2]. Note that the adamantane cores in **3**·AcOH have *van-der-Waals* contact, since the length of the vector between two opposite tetracarboxylic acids of a super-adamantane unit (along which the three diamond lattices may be translationally merged into one another) amounts just to about three times the diameter of an adamantane core. However, note also that the twofold interpenetration derived from the threefold interpenetration of **3**·AcOH by removing one super-diamond lattice would correspond *exactly* to the asymmetric twofold interpenetration present in **4**·TBB only, if the asymmetry shift vector of the latter were parallel to the cell edge *c*. In actual fact, the asymmetry shift vector ($0.136\mathbf{a} + 0.124\mathbf{c}$; see above) of **4**·TBB approximately runs along an *a*, *c* face diagonal (*Fig. 12*). This is particularly clearly brought about by the stereoviews of *Fig. 13b*, and we are at last left with the task to analyze the specific shape of the cavities opening up in the host architecture of **4**·TBB.

To evaluate the shape of the host cavities in **4**·TBB, the various space-filling stereoviews provided by *Fig. 13* are helpful. It may be seen from the diagrammatic representation of *Fig. 13b* that the asymmetry shift vector is practically parallel to a '1,3 distance' (perpendicular to the monoclinic *b* axis) of a super-adamantane unit. This leads to the perception that rather wide channels should open up with channel axes perpendicular to both the asymmetry shift vector and the crystallographic *b* axis. The space-filling view of *Fig. 13c* is projected orthogonal to these two axes and shows pretty impressively that this is indeed the case: the channels opened up through the asymmetry shift have a rather substantial cross-section with a rough diameter of *ca.* 7.5 Å! Thus the crude adamantane bulk limit derived above for guest molecules to break the double-diamond-like host structure of **4** in favor of an extremely hollow single-diamond-like host lattice appears

substantiated. Closer inspection of the space-filling views of *Fig. 13* shows that the wide host channels in **4**·TBB involve bottle-necks of some size, which are represented by the bulky adamantane cores (and, in particular, by the CH_2= groups protruding into the channels) of the molecules **4**.

The wide, somewhat bottle-necked channels in **4**·TBB as defined above would be present also if both diamond-like host lattices were interpenetrating symmetrically. However, as already indicated above, in that case we would have these channels in doubled number with about halved cross-section. This is precisely the situation in the symmetrically interpenetrating double-diamond-like host architectures of **4**·(MP-DMH-M), **4**·M_2, and **4**·(MP-M) described earlier. Comparison of the fully analogous space-filling views of *Fig. 3c* (**4**·(MP-DMH-M)) and, in particular, *Fig. 8d* (**4**·M_2) with that of *Fig. 13c* (**4**·TBB) provides lucid illustration. The final outcome of our analysis of the cavity characteristics in **4**·TBB may now be stated with particular clarity and simplicity: the asymmetry shift parallel to a 1,3 distance of a super-diamond lattice in **4**·TBB induced by the steric bulk of the TBB guest molecules leads to a twofold widening of one half of the host channels perpendicular to the shift vector (and the crystallographic *b* axis) at the expense of the other half of the channels, whose cross-section is reduced to zero (all-or-nothing principle, see above; compare *Figs. 13c* and *d* with *Figs. 3c* and *8d*). However, it is to be noted in conclusion that the walls of the expanded channels in **4**·TBB are not tightly closed yet have elliptical holes, which appear large enough to house portions (Ph rings) of the TBB guest molecules (*Figs. 13b* and *d*). These holes in the channel walls open up between the relatively slim COOH linkages and may be understood as remnants of a set of channels, which in **4**·(MP-DMH-M), **4**·M_2, and **4**·(MP-M) run orthogonal to those becoming widened by the asymmetry shift. These orthogonal, hole-producing channels are not affected by the asymmetry shift. Their existence simply follows from the tetragonal crystal symmetry of these three host-guest complexes inasmuch they run perpendicular to the tetragonal *c* axis. In fact, one would expect them to still show up in **4**·TBB relatively unchanged through rotating the view of *Fig. 13c* around the vertical (monoclinic) axis by 90°. This operation produces the view shown in *Fig. 13d*, which indeed exhibits the expected close similarity with the corresponding views of *Fig. 3c* and, in particular, *Fig. 8d* applying to the tetragonal cases.

Since the sterical bulkiness of TBB is not much smaller than the adamantane bulk limit qualitatively deduced above, some further attempts to enforce a single-diamond architecture of host **4** were pursued by offering guest species still more voluminous than TBB (see also *Experimental*). To offer an excess of guest material as large as possible, bulky guests were tried, which are themselves liquids. The necessarily relatively low crystallization tendency (low lattice energy) of such liquids is expected to provide an additional incentive for entering into inclusion compounds. The inclusion of solid bulky guest molecules would appear to require a particularly good tuning of host and guest molecular shapes, which is difficult to anticipate by systematic reasoning for an inclusion compound with guest cavities as large as those envisaged here (*cf.* above). A typical, fairly straightforward example tried was a non-stoichiometric inclusion compound of **4** with (*tert*-butyl)cyclohexane as guest, the crystals of which had cell constants almost identical with those of **4**·TBB, and which thus very probably also have a (asymmetric) double-diamond-like host structure (see *Experimental*). So far, we have not been able to produce experimental evidence in favor of a single-diamond-like inclusion compound of **4**, but

experimenting towards this challenging goal continues in our laboratory. However, irrespective of whether or not such an inclusion compound with an extremely high fraction of guest molecules can eventually be turned into reality, we may note in conclusion that on the whole our original conception of conferring inclusion propensity on adamantanetetracarboxylic acid **1** by introducing two CH_2= groups playing the role of steric perturbators as in **4** was rather successful. As a matter of fact, so much so that in a way it does not seem exaggerated too much to refer to **4** as an 'organic zeolite'.

5. *Structural Dichotomy of the Monohydrate of* **4** (**4**·H_2O): *Cross-Linked Double-Zincblende Architecture* vs. *Cross-Linked Concatenated Double-Sheet Structure.* As noted in the *Introduction*, the present tetrahedral dimethylidenetetra-acid **4** forms a very stable monohydrate (**4**·H_2O), which was also subjected to detailed X-ray analysis. A description of the crystal structure of **4**·H_2O is appended to the present report as a concluding section, since this hydrate turned out to involve double-diamond-like features. Alternatively, the crystal structure of **4**·H_2O may be characterized in terms of concatenated, doubly interpenetrating molecular sheets, which will finally be outlined in some detail.

The monohydrate **4**·H_2O crystallizes triclinic in the centrosymmetric space group $P\bar{1}$ with 4 molecules of **4** and 4 H_2O molecules in the unit cell. The asymmetric unit consists of two non-equivalent tetra-acid and H_2O molecules each, which have no crystallographic symmetry, of course. No disorder phenomena are perceptible in the crystal structure of **4**·H_2O. Both independent tetracarboxylic-acid molecules of the hydrate are structurally similar with respect to one another (*Fig. 14*) and also resemble the four tetra-acid geometries observed in the inclusion compounds discussed above. The conformation of the COOH groups is again such that steric interference with the CH_2= groups is avoided, *i.e.* the COOH and C=C bond planes are more or less orthogonal. However, *Fig. 14* shows that significant deviations from these symmetric dispositions occur in the hydrate **4**·H_2O, which are larger than encountered in the inclusion compounds **4**·(MP-DMH-M), **4**·M_2, **4**·(MP-M), and **4**·TBB. In addition, *Fig. 14* also shows that the locations of the COOH H-atoms in **4**·H_2O do not conform to approximate D_2 symmetry. These enhanced asymmetries of the tetra-acid in the hydrate are probably of some significance as a cause for slight pyramidalizations observed at the olefinic C(sp^2)-atoms of the adamantane cores. Finally, it is pointed out once again that the C=C bonds of **4** are shortened also in the present hydrate **4**·H_2O (by *ca.* 0.02 Å; *Fig. 14b*), probably chiefly due to thermal motion; compare the four inclusion compounds of **4** described above, in which this effect is also observed. We do not discuss intramolecular structural details of **4**·H_2O any further; basic results of the structure refinement are reproduced in *Table 6* and *Fig. 14*.

As may be expected from the low crystal symmetry of **4**·H_2O, its pattern of H-bonding is rather complex (*Fig. 15*). However, the analysis of the H-bond architecture of **4**·H_2O is facilitated by the observation that the H-bonding environments around both independent tetra-acid molecules (*Fig. 16a*) are very similar; likewise, the patterns of H-bonding around both independent H_2O molecules (*Fig. 16b*) agree closely. In accord with the ordered nature of the crystal structure of **4**·H_2O, no H-bonding occurs across centers of symmetry. (Of course, the uncharged O(H)O H-bonds of **4**·H_2O are clearly asymmetric.) It is noted that the COOH groups of the tetra-acid molecules of **4**·H_2O are in no case linked by the usual pairwise H-bonds as found in the four inclusion compounds of **4** described above. Instead, the four COOH groups of every tetra-acid molecules are

connected to COOH groups of four different tetra-acids in a severely distorted tetrahedral fashion by means of *single* O(H)O H-bonds (*Figs. 16a* and *18a*). The second O-atom of each COOH group is H-bonded to a H_2O O-atom such that the tetra-acid molecules in **4**·H_2O are coordinated to four different H_2O molecules in a comparatively little distorted tetrahedral disposition (*Figs. 16a* and *17*). All H–O–C=O groupings of the COOH groups adopt the energetically favorable synplanar partial conformation. It may be seen from *Figs. 15*, *16* and *18a* that the single H-bonds between the COOH groups are of two different kinds. One half of these linkages relate COOH groups with approximately antiparallel C–C(OOH) bonds (*Fig. 16d*), while the other half connects markedly tilted COOH groups (*Fig. 16c*). Two non-equivalent COOH···COOH (intercarboxylic) H-bonds of both these types occur, which have O(H)O distances of 2.662, 2.667 (antiparallel) and 2.613, 2.635 Å (tilted), respectively (estimated standard deviations, 0.002 Å).

Four H-bonds emanate from each H_2O O-atom of **4**·H_2O with rather well approximated tetrahedral directionality. They connect the H_2O molecules with COOH groups of four different tetra-acid molecules. *Fig. 16b* exemplifies that the H-bonds protruding from the H_2O molecules basically fall into two classes: two of these linkages extend towards COOH groups which are engaged in the above-mentioned 'tilted' intercarboxylic H-bonds, and the other two towards COOH groups involved in 'antiparallel' intercarboxylic H-bonds. In the former case a H-bridged seven-membered C,O ring is formed, which has previously been observed *e.g.* in the crystals of hydrates of benzene-1,3,5-tricarboxylic acid (trimesic acid, TMA) [17] and in the monohydrate of pyridine-2,6-dicarboxylic acid [18]. Altogether 8 non-equivalent H-bonds between the H_2O molecules and the tetra-acid COOH groups are present in the crystals of **4**·H_2O, four of each of the two classes characterized above. The observed associated O(H)O distances are 2.737, 2.793, 2.853, 2.890 (average 2.82) and 2.694, 2.718, 2.774, 2.778 (average 2.74) Å between H_2O and the 'tilted' and 'antiparallel' COOH groups, respectively (estimated individual standard deviations, 0.002 Å).

The supramolecular H-bonded architecture of the crystals of **4**·H_2O, which on first sight appears rather complex (*Fig. 15*), was analyzed computer-graphically by preparing two series of stereo plots of eight unit-cell contents. In the first series, only the H-bonds between H_2O and the COOH groups were drawn, and in the second series exclusively those between the COOH groups themselves. The first graphics series revealed that the three-dimensional network of H-bonded tetra-acid and H_2O molecules of **4**·H_2O may convincingly be characterized in terms of a distorted double-diamond structure. Alternatively, the second series of plots indicated that the H-bonded tetra-acid molecules may also be grouped into two 4-connected two-dimensional networks interpenetrating each other and leaving open cavities, which accommodate the H_2O molecules. The final paragraphs of this report are devoted to a discussion in some detail of these two attractive possibilities of viewing the molecular packing in **4**·H_2O.

As a general overview, *Fig. 15* provides a stereoscopic space-group symmetry diagram, which outlines the contents of 8 unit cells including the cell edges. The two symmetry-independent tetra-acid and H_2O molecules are differentiated as of *Type 1* and *Type 2*, respectively. Analyzing *Fig. 15*, one may identify H-bonded double layers in planes parallel to the crystallographic *a,b* plane formed exclusively by *Type 1* tetra-acid and H_2O molecules (around $x, y, 1/2$), and adjacent parallel ones built up only by *Type 2* molecules (around $x, y, 0$). The double layers consisting alternatingly either of *Type 1* or

of *Type 2* molecules are obviously not symmetry-related. Within the double layers, the constituting single layers are related by centers of symmetry, yet are not linked by H-bonds. The COOH···COOH H-bonds within the two layers of one and the same double layer are of the tilted variant, whereas those of the antiparallel variant connect layers belonging to different, adjacent double layers (*Fig. 15*). It is noted parenthetically that the C=C bonds are approximately all oriented parallel in the crystals of **4**·H_2O.

The layers of tetra-acid and H_2O molecules parallel to the *a*, *b* plane referred to above are built up of fused 'super-cyclohexane chairs' formed by alternating centers of H-bonded tetra-acid and H_2O molecules. The two puckered super-cyclohexane sheets of a particular double layer now are linked to similar sheets of the two adjacent double layers *via* H_2O···COOH H-bonds, such that two interpenetrating super-diamond architectures result. In fact, the analogy with zincblende ZnS (sphalerite) is even closer. More specifically, we may accordingly state that the H_2O···COOH H-bond system in **4**·H_2O is that of a distorted double super-zincblende structure, in which *e.g.* the Zn-atoms are replaced by tetrahedrally coordinated H_2O molecules and the S-atoms by the tetrahedral molecules **4**. Every tetra-acid molecule is tetrahedrally H-bonded to 4 H_2O molecules, and every H_2O molecule is bonded likewise to 4 tetra-acid molecules. Both interlaced super-zincblende networks in **4**·H_2O are composed of 50% *Type-1* and 50% *Type-2* molecules, and are equivalent across centers of symmetry.

As mentioned, the double-zincblende description of **4**·H_2O is defined by the H-bonds between the H_2O molecules and the tetra-acid COOH groups. One half of the single COOH···COOH H-bonds, namely those of the tilted nature, also fit into the double-zincblende picture inasmuch they occur within one and the same super-zincblende framework. However, the antiparallel COOH···COOH H-bonds interconnect different super-zincblende networks, so that we finally may refer to **4**·H_2O as being structured according to a cross-linked double-zincblende architecture. We may thus conclude that five sixth of all the H-bonds of **4**·H_2O can be assigned to the two super-zincblende networks, and that one sixth represent cross-links between the two networks. It is clear that two different super-adamantane units may be cut out of a super-zincblende network, one consisting of 4 tetra-acid and 6 H_2O molecules, and another one composed of 6 tetra-acid and 4 H_2O molecules (*Fig. 17a*). The molecule of an interpenetrating network sitting in the center of a super-adamantane cage is always of the same kind as the 4 molecules representing the 'bridgeheads' of the super-adamantane cage. *Fig. 17* provides various stereoviews illustrating the beautiful interlaced double-zincblende architecture of **4**·H_2O. We note finally that ammonium perrhenate NH_4ReO_4 [19] provides another, higher symmetric example (tetragonal space group $I4_1/a$) of a H-bonded double super-zincblende structure with alternating $NH_4^{\oplus}$ and $ReO_4^{\ominus}$ tetrahedral centers.

Whereas the double-diamond-like nature of the crystal structure of **4**·H_2O evolves from focussing the packing analysis on the H_2O···COOH H-bonds, emphasizing the COOH···COOH H-bonds brings about a second interesting facet of this hydrate's structural dichotomy. The COOH···COOH H-bonds join the tetra-acid molecules in such a way that distorted tetragonal sheets come about, which are heavily corrugated (puckered) and consist of large fused 'super-cyclobutane' rings. Within these 4-connected two-dimensional nets the tilted and antiparallel intercarboxylic H-bonds referred to above very roughly run in perpendicular directions. As an analogy, the crystal structure of H_2SO_4 may be cited [20], the H-bond pattern of which may also be characterized on the

basis of simple 4-connected plane nets (non-interpenetrating). Stereo-illustrations of this neat pattern of H-bonding in **4**·H_2O are provided by *Fig. 18*, which should also be duly inspected in conjunction with the following discussion. The super-cyclobutane rings built up by the COOH···COOH H-bonded tetra-acid molecules have central holes, which are filled by a second interpenetrating corrugated sheet of H-bonded tetra-acid molecules. We are thus faced with interlaced double layers, and the crystal structure of **4**·H_2O may be viewed as a stack of such pairwise interlocking sheets with the H_2O molecules intercalated between the double layers.

Like the super-zincblende networks referred to above, the individual super-cyclobutane sheets of **4**·H_2O are composed of 50% *Type 1* and 50% *Type 2* tetra-acid molecules. The two sheets forming a concatenated double layer are symmetry-equivalent across centers of symmetry, while the stacked double layers may be merged into one another by simple elementary translations (*Fig. 18*). The interwoven double layers are held together in the crystal by the H_2O molecules acting as a cross-linking 'cement' *via* 4 tetrahedral H-bonds protruding from each H_2O O-atom towards COOH O-atoms of four different tetra-acid molecules (see super-zincblende description above). Quite obviously, the crystal structure of **4**·H_2O also involves characteristics of a solid-state inclusion or intercalation compound with the stacked interlaced tetra-acid double layers playing the role of the host architecture and the H_2O acting as molecular guest. One third of the H-bonds, *i.e.* the COOH···COOH linkages, are defined within the interlaced double layers and two thirds, *i.e.* the H_2O···COOH linkages, are engaged in cross-linking (*Fig. 18*).

Rather similar H-bonded super-cyclobutane rings as in **4**·H_2O occur in various hydrates of trimesic acid (TMA) involving TMA·H_2O layers [17]. However, the antiparallel single H-bonds between the COOH groups in **4**·H_2O are replaced by the usual pairwise COOH···COOH H-bonds in the TMA·H_2O sheets. Furthermore, the open-meshed TMA·H_2O sheets do not interpenetrate yet are stacked on top of each other to form channels, which are occupied by guest molecules (additional H_2O or TMA molecules, or foreign guests such as picric acid [17]).

The structural motif of interpenetrating, concatenated two-dimensional networks is rather rare in crystal chemistry so that it appears appropriate to conclude the discussion of the crystal structure of **4**·H_2O by briefly highlighting three known comparable cases. H_2O-free TMA forms puckered, hexagonal 'super-graphite' sheets in the crystal by means of pairwise H-bonds between the COOH groups [7]. The 'super-benzene' rings of these sheets have very large central holes filled by super-benzene rings of three interpenetrating, symmetry-equivalent sheets (*Fig. 19a*). Owing to the larger hollowness of the pleated hexagonal sheets of TMA, the degree of interpenetration is thus altogether fourfold, as compared to the twofold interpenetration of the corrugated tetragonal sheets in **4**·H_2O.

A closer analogy with our present hydrate is provided by the Ag salt of cyanoform $Ag[C(CN)_3]$, which also forms pairwise interpenetrating, puckered hexagonal super-graphite sheets in the crystal (trigonal coordination of Ag by N) [8]. The puckering mode of the individual sheets is essentially that of black phosphorus [21] such that the individual sheet structure of $Ag[C(CN)_3]$ may more aptly be characterized as a 'super-black phosphorus' architecture. The super-cyclohexane rings of the Ag complex are smaller than the super-benzene rings in TMA such that twofold interpenetration suffices to fill the holes. Two interpenetrating sheets constitute a double layer, and the crystal consists of a

stack of such double layers (*Fig. 19b*) much like in our present structure of $4 \cdot H_2O$. Of course, a difference between the two cases ensues from the fact that the stacked interlaced double layers of $Ag[C(CN)_3]$ are not cross-linked by intercalated (guest) molecules.

The third example relevant in our context concerns *Hittorf*'s (monoclinic) phosphorus, the complex yet beautiful polymeric structure of which may also be characterized in terms of double layers of two interpenetrating macromolecular, two-dimensional networks [9]. Actually, in essence the individual phosphorus sheets are tetragonal 4-connected nets as in $4 \cdot H_2O$ (*Fig. 19c*). However, the interlaced double layers of *Hittorf*'s phosphorus are again not cross-linked, in contradistinction to $4 \cdot H_2O$. The fascinating topologies of the interpenetrating networks present in TMA, $Ag[C(CN)_3]$, and *Hittorf*'s phosphorus (as well as in $4 \cdot H_2O$ and the double-diamond-like inclusion compounds presented further above) can only properly be appreciated by suitably designed stereodrawings. Since no appropriate illustrations of this kind have appeared in the literature, diagrammatic stereoviews have been prepared from the published atomic coordinates of these three structures; they are shown in *Fig. 19* and may instructively be compared to the corresponding *Fig. 18* applying to $4 \cdot H_2O$.

Financial support of the *Fonds der Chemischen Industrie* is gratefully acknowledged.

REFERENCES

[1] O. Ermer, *J. Am. Chem. Soc.* **1988,** *110,* 3747.
[2] O. Ermer, L. Lindenberg, *Helv. Chim. Acta* **1988,** *71,* 1084.
[3] J. L. Hoard, R. E. Hughes, D. E. Sands, *J. Am. Chem. Soc.* **1958,** *80,* 4507.
[4] a) R. Bishop, I. G. Dance, S. C. Hawkins, *J. Chem. Soc., Chem. Commun.* **1983,** 889; b) R. Bishop, I. Dance, *ibid.* **1979,** 992; I. G. Dance, R. Bishop, S. C. Hawkins, T. Lipari, M. L. Scudder, D. C. Craig, *J. Chem. Soc., Perkin Trans. 2* **1986,** 1299; I. G. Dance, R. Bishop, M. L. Scudder, *ibid.* **1986,** 1309; c) R. Bishop, S. Choudhury, I. Dance, *ibid.* **1982,** 1159; d) G. E. Bacon, R. S. Pease, *Proc. R. Soc. London, [Ser.] A* **1955,** *230,* 359; see also [14]; e) O. Ermer, M. Schank, to be published.
[5] S. Nishikiori, T. Iwamoto, Y. Yoshino, *Chem. Lett.* **1979,** 1509; S. Nishikiori, T. Iwamoto, *J. Incl. Phenomena* **1985,** *3,* 283.
[6] D. J. Haas, S. A. Brenner, *Acta Crystallogr.* **1966,** *20,* 709.
[7] D. J. Duchamp, R. E. Marsh, *Acta Crystallogr., Sect. B* **1969,** *25,* 5.
[8] J. Konnert, D. Britton, *Inorg. Chem.* **1969,** *5,* 1193.
[9] H. Thurn, H. Krebs, *Acta Crystallogr., Sect. B* **1969,** *25,* 125.
[10] J. Donohue, 'The Structures of the Elements', Krieger, Malabar, Florida, 1982, pp. 48–56.
[11] 'Gmelin Handbook of Inorganic Chemistry', 8th edn., Springer, Berlin–Heidelberg–New York, 1981, Syst.-No. 13 (Boron), Suppl. Vol. 2, pp. 58–70.
[12] 'International Tables for Crystallography', 'Space-Group Symmetry', Ed. Th. Hahn, Reidel, Dordrecht, 1983, 1987, 1989, Vol. A.
[13] H. Bärnighausen, *MATCH-Commun. Math. Chem.* **1980,** *9,* 139.
[14] O. Ermer, A. Eling, *Angew. Chem. Int. Ed.* **1988,** *27,* 829.
[15] F. H. Allen, O. Kennard, R. Taylor, *Acc. Chem. Res.* **1983,** *16,* 146.
[16] G. Bergerhoff, R. Hundt, R. Sievers, I. D. Brown, *J. Chem. Inf. Comput. Sci.* **1983,** *23,* 66; D. Altermatt, I. D. Brown, *Acta Crystallogr., Sect. B* **1985,** *41,* 240; I. D. Brown, D. Altermatt, *ibid.* **1985,** *41,* 244.
[17] F. H. Herbstein, R. E. Marsh, *Acta Crystallogr., Sect. B* **1977,** *33,* 2358; see also: F. H. Herbstein, *Topics Curr. Chem.* **1987,** *140,* 107.
[18] F. Takusagawa, K. Hirotsu, A. Shimada, *Bull. Chem. Soc. Jpn.* **1973,** *46,* 2020.
[19] G. J. Kruger, E. C. Reynhardt, *Acta Crystallogr., Sect. B* **1978,** *34,* 259.
[20] C. Pascard-Billy, *Acta Crystallogr.* **1965,** *18,* 827.
[21] A. Brown, S. Rundquist, *Acta Crystallogr.* **1965,** *19,* 684; R. Hultgren, N. S. Gingrich, B. E. Warren, *J. Chem. Phys.* **1935,** *3,* 351.